POLOIDAL OHMIC HEATING

IN A MULTIPOLE

by

Donald Joseph Holly

A thesis submitted in partial fulfillment

of the requirements for the degree of

DOCTOR OF PHILOSOPHY

(Physics)

at the

University of Wisconsin - Madison

1982

POLOIDAL OHMIC HEATING

IN A MULTIPOLE

Donald Joseph Holly

(Under the supervision of Professor J.C. Sprott)

The feasibility of using poloidal currents to heat plasmas confined by a multipole field has been examined experimentally in Tokapole II. The machine is operated as a toroidal octupole, with a time-varying toroidal magnetic field driving poloidal plasma currents $I_{plasma} \sim 20$ kA to give densities $n_e \sim 10^{13}$ cm^{-3} and temperatures $T_e \sim 30$ eV.

The measured plasma resistivity ranges from $\sim\eta_{Spitzer}$ to $\sim 1500 \times \eta_{Spitzer}$ and scales like $\sqrt{T_e}/n_e$ as expected from mirror- and fluctuation-enhanced resistivity theory. The enhanced resistivity allows large powers ($\sim$2 MW) to be coupled to the plasma at modest current levels. However, the poloidal ohmic heating reduces the confinement time from $\sim$ 1 msec to $\sim$30 μsec. This is apparently due to a combination of the unfavorable location of the input

power near the wall of the vacuum tank and fluctuation-enhanced transport.

A one-dimensional transport code calculation shows that the location of the input power near the walls yields a confinement time four to ten times shorter than if the power were deposited on the octupole separatrix.

The heating produces large ($\delta n/n \sim 100\%$) low-frequency ($f \lesssim 10$ kHz) fluctuations which are apparently current-driven. Local electric field measurements corellated with local density measurements show that these fluctuations further degrade the confinement time by a factor of two to five. Current-driven drift instabilities and resistive MHD instabilities appear to be the most likely causes for the fluctuations.

J. C. Sprott

ACKNOWLEDGMENTS

I would like to express my thanks to a number of people with whom I have had the honor of being involved in the course of this research.

J.C. Sprott suggested the research topic and shared valuable physical insight.

Discussions with S. Prager have been very helpful, and I thank him for his suggestions and encouragement. Discussions with T. Osborne, J. Callen, and D. Brouchous have also been of much help.

R. Dexter and N. Brickhouse provided measurements of impurity radiation and optical measurements of electron temperature. H. Garner and M. Phillips provided computer programs used in this research.

R. Vallem and the staff of hourly employees constructed and maintained much of the experimental equipment. The microwave interferometer was designed and constructed with the help of A. Hillery, T. Kruzel, and D. Witherspoon. I am indebted to T. Lovell for advice and encouragement on a great variety of subjects.

The tolerance of my office-mate J. Twichell and his help in preparing this manuscript is appreciated.

I am deeply thankful to Lorraine Gardner for her patience, love, and support.

Financial support for my research was provided by the AEC, ERDA, and DOE.

Table of Contents

PLP REPORTS

In this thesis, a number of references are made to the internal reports of the University of Wisconsin Plasma Physics Group. These reports, which are identified by PLP numbers, are available upon request from:

Plasma Physics Office
University of Wisconsin
1150 University Avenue
Madison, Wisconsin 53706

CHAPTER ONE: INTRODUCTION

Multipoles were among the first devices to stably confine plasmas,[1,2] but traditionally they have been operated with low-density, low-temperature plasmas. Recently, however, multipole plasmas have been pushed to higher densities and temperatures, both for general plasma studies and for assessment as advanced fuel reactors. While tokamak-like toroidal ohmic heating has been the more common technique used to heat multipole plasmas,[3,4] poloidal ohmic heating may offer several advantages, including enhanced resistivity due to the strong multipole magnetic mirrors; also, it is not known whether a current limit exists for this type of heating. This paper will describe poloidal ohmic heating experiments performed on Tokapole II (operated as an octupole) to determine the method's suitability as a plasma heating scheme.

Multipole fusion reactors[5,6] using advanced fuels such as p-^{6}Li or p-^{11}B would have several advantages over D-D or D-T reactors, based on the fact that the advanced fuel reactions produce few or no neutrons. The absence of neutron damage to materials and the fact that no fuel breeding would be needed (as it would for a D-T reactor) would greatly simplify blanket design, removing one of the major difficulties in fusion reactor design. Elimination or reduction of the neutron flux means that advanced fuel reactors could also offer improved maintainability and would be environmentally more desirable than D-T or D-D fusion reactors.

Advanced fuels typically require much higher temperatures for ignition than D-T or D-D. Typical design temperatures range from 50 to 300 keV for advanced fuels, compared to the 10 to 20 keV needed for a D-T reactor. The p-^{11}B cycle has not been fully explored and it is not certain whether its Q (defined as the fusion power divided by the injected power) can be made greater than one.[6,7] p-^{6}Li looks more promising;[8] early calculations showed that its Q would be limited to about 3, but a more detailed calculation,

taking into account nuclear scattering, propagation reactions, and the interactions between the particles in the high-energy tails of the energy distributions, indicates that higher Q's might be obtained. For example, at $T_i \sim 250$ keV, $T_e \sim 155$ keV, a Q of 32 may be possible.[9]

These high temperatures are typical of those required for burning advanced fuels, and are the reason that multipoles appear uniquely suited for advanced fuel reactors. At these high temperatures synchrotron radiation losses become excessive unless the magnetic field is very small; multipoles have the unusual ability to operate with a large internal low-field region. This ability makes multipoles attractive for burning advanced fuels, despite the engineering difficulties such as cooling and levitating the internal rings. Similarly, advanced fuels are uniquely suited for burning in multipole reactors, since the low neutron yield is necessary to minimize damage to the internal rings.

Present-day multipoles typically run near $n = 10^{12}$ cm^{-3}, $T_e = 10$ eV; multipole reactors would require something like $n = 10^{14}$, $T_e = 150$ keV, $T_i = 300$ keV. As a step toward scaling multipole parameters toward reactors, a Proof-of-Principle (POP) multipole/Surmac experiment has been proposed by TRW, UW, and UCLA.[9,10] This would be a $28 million octupole with levitated superconducting rings, and would be about 1.5 m in major radius, with fields of about B = 20 kG, $n = 10^{14}$ cm^{-3}, and $T_i = T_e = 1$ keV. The plasma would be heated with poloidal ohmic heating to about 100 eV, then raised to its final temperature using neutral beam injection.

While the proposal study concluded that poloidal ohmic heating was technologically the most straightforward startup method for the POP octupole design, it also called for more investigation of the effects of poloidal ohmic heating: "The viability of poloidal ohmic heating has been established experimentally. The only deleterious effect observed so far is a reduction of energy confinement, possibly associated with the presence of current-driven drift

waves. Stability against filamentation, kink and sausage modes, etc., will be determined."[9]

Besides its potential for heating reactors or multipole proof-of-principle devices, poloidal ohmic heating may prove useful in pushing present-day multipole plasmas into new regimes. Multipoles have some interesting features as plasma research facilities, such as the ability to confine plasma without a sheared magnetic field and the ability to operate at a high β (the Wisconsin Levitated Octupole has recently been operated at a β of 35%).[11] Poloidal ohmic heating was the first ohmic heating applied to the original Wisconsin Octupole, but was soon replaced with toroidal ohmic heating, and was never thoroughly studied.

The research described here addresses a number of questions pertaining to poloidal ohmic heating in a multipole as a plasma heating scheme. Among these questions are:

*Does poloidal ohmic heating couple significant amounts of power into a multipole plasma?

*What is the poloidal resistivity? Do the magnetic mirrors enhance it above Spitzer resistivity as expected from mirror-enhanced resistivity theory?

*Is the input power converted to thermal plasma energy?

*What is the poloidal current limit?

*Does poloidal ohmic heating alter the multipole's MHD equilibrium or stability?

*Does it produce other loss enhancement over a standard multipole configuration?

The answers should be relevant both to general plasma studies in multipoles and to advanced fuel multipole reactors.

REFERENCES FOR CHAPTER ONE

1. T. Ohkawa and D.W. Kerst, Phys. Rev. Letters 7, 41 (1961)

2. R.A. Dory, D.W. Kerst, D.M. Meade, W.E. Wilson, and C.W. Erickson, Phys. Fluids 9, 997 (1966)

3. A.P. Biddle, R.N. Dexter, R.J. Groebner, D.J. Holly, B. Lipschultz, M.W. Phillips, S.C. Prager, and J.C. Sprott, Nuclear Fusion 9, 1509 (1979)

4. P.I. Peterson, C.J. Armentrout, C.J. LaHaye, and R.D. Stambaugh, Bull. Am. Phys. Soc. 23(7), 835 (1978)

5. F.F. Chen, UCLA PPG-553 (1981)

6. R.W. Conn, G.W. Shuy (UCLA); D. Kerst, I.N. Sviatoslavsky, D.K. Sze (University of Wisconsin); D. Arnush, A.J. Cole, J.D. Gordon, L. Heflinger, T. Samec, W. Steele (TRW); C.C. Baker, A. Bolon, R.G. Clemmer, J. Jung, D.L. Smith (Argonne Laboratory); G.

Miley, T. Blue, J. DeVeaux, D. Driemeyer, J. Gilligan, J. Metzger, W. Tetley (University of Illinois, Urbana), 8th International Conference on Plasma Physics and Controlled Nuclear Fusion Research, Brussels, Belgium, July 1-10 1980, paper IAEA-CN-38/V-5

7. G.W. Shuy and R.W. Conn, UCLA PPG-522 (1980)

8. G.W. Shuy, UWFDM-335 (1979)

9. University of California at Los Angeles, University of Wisconsin, TRW Defense and Space Systems Group, "A Proof-of-Principle of the Advanced Fuels Multipole-Surmac Concept," prepared for the Department of Energy, Office of Magnetic Fusion Energy (October 1978)

10. D. Arnush, R. Conn, J.M. Dawson, B. Fried, D. Kerst, T. Samec, V. Vanek, A.Y. Wong, "Multipole Fusion Reactors Using Advanced Fuels," in Proceedings of the Review Meeting on Advanced Fuel Fusion, EPRI ER-536-SR (1977), pp. 103-121

11. J.H. Halle, A. Kellman, R.S. Post, S.C. Prager,

E.J. Strait, M.C. Zarnstorff, University of Wisconsin Plasma Physics Report DOE/ET53051/9 (1980)

CHAPTER TWO: THE MACHINE

A. TOKAPOLE II

Tokapole II [1,2,3] (Figure 2-1) is a pulsed toroidal plasma device which may be run either as a tokamak with a four-node poloidal divertor or as a toroidal octupole. In the experiments to be described, it was operated as a toroidal octupole.

The vacuum chamber is of aluminum with major radius 50 cm and square cross section 44 cm x 44 cm. The walls are 3 cm thick, so that field soak-in to the walls is small on the few millisecond time scale of the experiment (the field soaks through the walls in about 15 msec). Because of this, insulated gaps are provided to allow the magnetic fields to enter the machine.

The poloidal field is provided by currents induced in four internal copper rings through an iron core transformer. Image currents flowing in the aluminum walls confine the field to the inside of the torus.

Figure 2-1. Tokapole II.

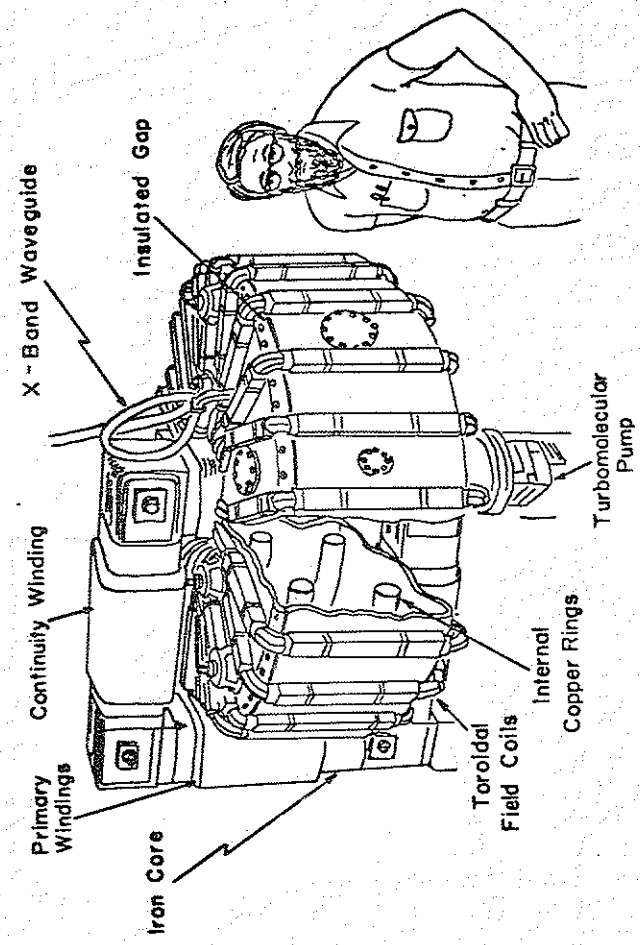

TOKAPOLE II

The poloidal electric field (and toroidal magnetic field) is produced by 24 sets of 4 wires each wound on the outside of the vacuum tank. To minimize field perturbations, the wires cross the toroidal gap at uniform intervals.

The vacuum is maintained by a 1500 l/s turbopump attached to a 7.5" port and a 1000 l/s 10 K cryopump which pumps through a 4.5" port. Base pressure is usually in the low 10^{-7} torr range. Taylor discharge cleaning,[4] or more recently, glow discharge cleaning[5] in H_2 is used to condition the walls when the machine is not being run.

B. FIELD TIMING

Figure 2-2 shows a typical sequence of events in a poloidal ohmic heating shot. H_2 gas is puffed into the machine through a piezoelectric puff valve. 10 msec later an ignitron fires a bank of thirty 240 μF 5 kV capacitors into the poloidal field primary windings, giving a pulse with a half-period of 5.8 msec. Shortly before peak poloidal field a 1 msec pulse of 8.8 GHz

Figure 2-2. Typical timing sequence for a poloidal ohmic heating shot in Tokapole II.

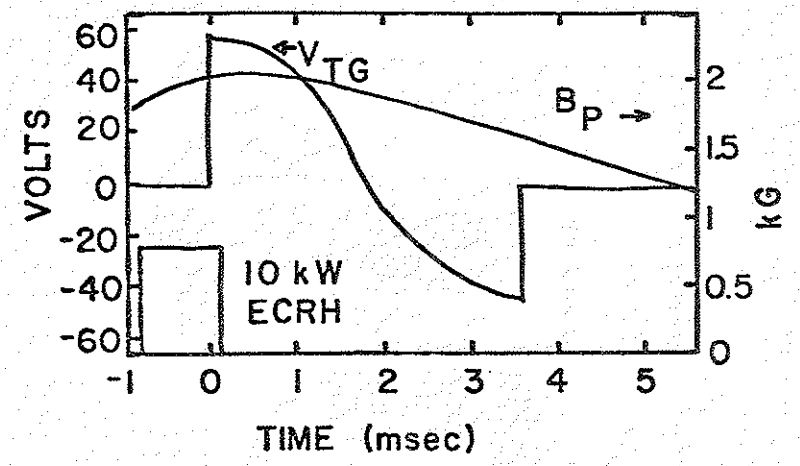

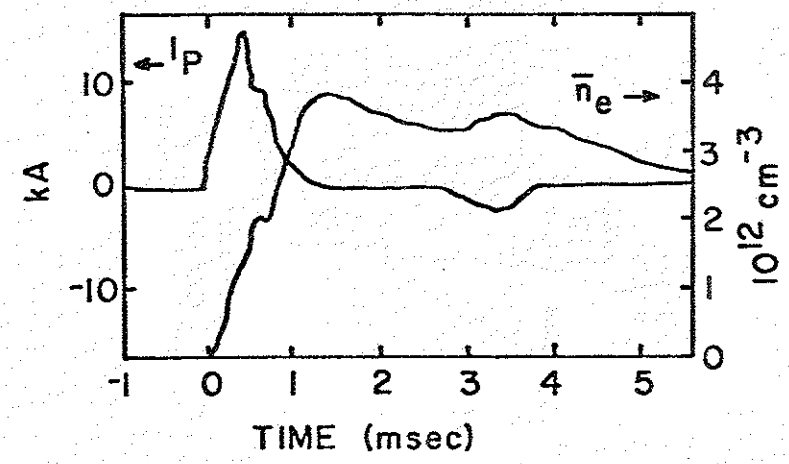

microwaves is used to preionize the plasma via electron cyclotron heating, giving a plasma with density $n_e \sim 10^{10}$ cm^{-3} and temperature $T_e \sim 10$ eV. When the poloidal field reaches its peak it is crowbarred, and the toroidal field is fired to give a poloidal electric field. Toroidal field turns ratios can be set at 96:1, 48:1, or 24:1 to give poloidal loop voltages up to about 200 V, although typically a poloidal loop voltage of about 60 V is used. A bank of twenty-four 240 μF 5 kV capacitors is used to create the toroidal field.

C. MAGNETIC FIELD STRUCTURE

Figure 2-3a, generated by the TORMESH[6,7] code, shows projections of surfaces of constant poloidal magnetic flux Ψ. The surfaces are labelled in normalized units from 0 (at the surface of the rings) to 10 (at the wall). Inside the separatrix (at $\Psi \sim 5$) flux surfaces link a single ring and are called private; outside the separatrix flux surfaces link all four rings and are called common. The critical flux surface Ψ_c is at $\Psi \sim 8.2$; flux surfaces inside of Ψ_c

Figure 2-3.a) Projections of constant poloidal flux surfaces in Tokapole II. The surfaces are labeled from 0 (at the rings) to 10 (at the wall). The separatrix is at $\Psi \sim 5$; the critical surface Ψ_c is at $\Psi \sim 8.2$.

$$\alpha = \frac{B_T}{B_P} \text{ (MPOW)}$$

Figure 2-4 shows M as a function of flux surface Ψ for various values of α. In the poloidal-ohmically-heated octupole α generally ranges from about .08 to about 1.6, so that the toroidal magnetic field is not insignificant compared to the poloidal field.

D. ELECTRIC FIELD

The poloidal field crowbar is able to hold the toroidal loop voltage to a few volts, and thus the electric field in this experiment is almost purely poloidal. This poloidal electric field is calculated by a computer program[8] from the equation

$$\vec{E}(\vec{x}) = -\frac{\partial}{\partial t}\vec{A}(\vec{x})$$

$$= -\frac{\partial}{\partial t}\frac{\mu_o}{4\pi}\int\frac{\vec{J}(\vec{x}')}{|\vec{x}-\vec{x}'|}\,dx'$$

Figure 2-4. Mirror ratio M as a function of Ψ for various values of $\alpha = (B_T/B_P)_{MPOW}$.

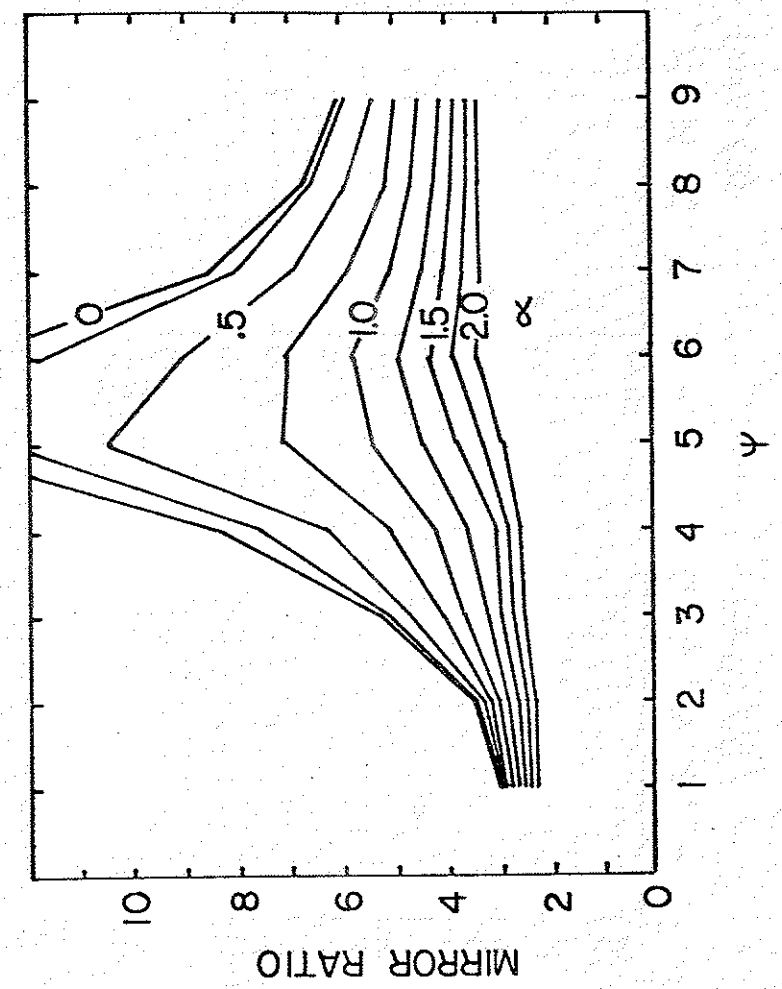

The program calculates the vacuum electric field by approximating the wall current (induced by the toroidal field windings) as a series of 24 poloidal filament currents. (The number 24 is chosen for convenience and is unrelated to the fact that there are 24 sets of toroidal windings.) The hoops are assumed to be perfect conductors; thus each hoop is assumed to carry a poloidal filament current equal and opposite to the wall filament at each azimuth. The program follows along poloidal flux surfaces, calculating the electric field at uniformly-spaced points and then summing components parallel to the flux surfaces to get the average electric field $\langle E_{\parallel}(\Psi)\rangle$ (Figure 2-5a). In figure 2-5b $\langle E_{\parallel}\rangle$ is plotted as a function of distance from the major axis for locations on the midplane. Note that the calculation gives the local value of $E_{\parallel}$ at points along the flux surfaces, but for most purposes only the averaged value will be important.

Figure 2-5.a) Average parallel electric field $\langle E_{||} \rangle$ vs. flux surface Ψ. The fields shown are for a B_T bank of 5760 μF charged to 1.5 kV with the B_T windings set at 48:1 turns ratio.

b) $\langle E_{||} \rangle$ plotted against distance from major axis on the midplane. The conditions are the same as in a.

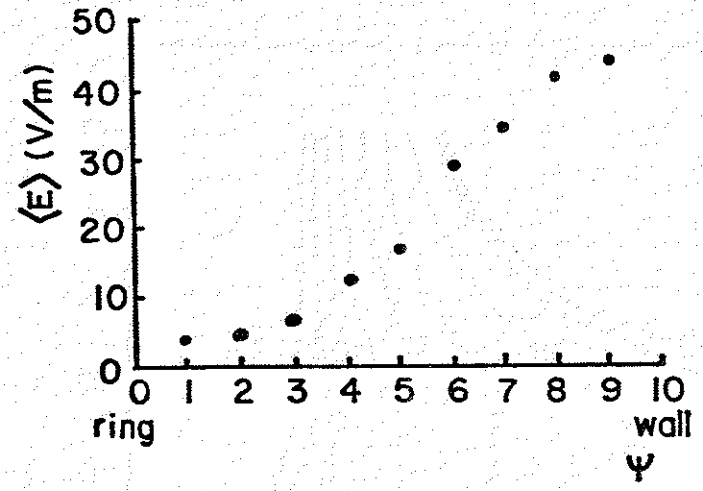

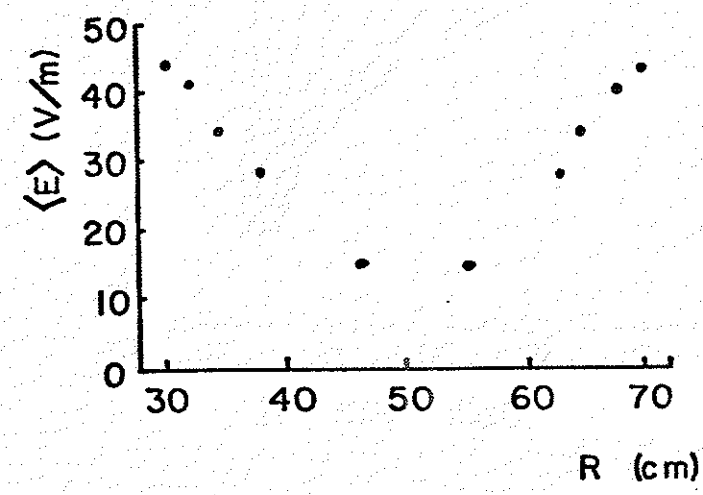

E. GENERAL PLASMA CHARACTERISTICS

The electron density produced by poloidal ohmic heating in Tokapole II typically ranges from 10^{11} cm^{-3} to a few times 10^{13} cm^{-3}. Initially the density is peaked toward the wall, where most of the ohmic heating takes place; the peak shifts inward toward the separatrix as the poloidal current dies away. The density typically peaks about a millisecond after the heating voltage is applied and decays with a time constant of a few milliseconds after the heating is turned off. Figure 2-6 shows a typical scan of ion saturation current taken on the midplane during poloidal ohmic heating. As shown in the figure, the ohmic heating is accompanied by large local density fluctuations, $\delta j_{sat}/j_{sat} \sim 100\%$; the fluctuation level is highest in the region where the current flows and falls to less than 10% after the heating is turned off.

Electron temperature ranges from a few eV to about 30 eV. As the ohmic input power is raised, the electron temperature increases until it reaches about 30 eV. Further increases in input power do not cause a significant increase in T_e. Figure 2-7 shows a typical

Figure 2-6.a,b,c) Ion saturation current and percent fluctuation in ion saturation current in midplane for various times after the poloidal electric field is applied. Toroidal bank voltage is 3.0 kV, poloidal bank voltage is 2.0 kV.

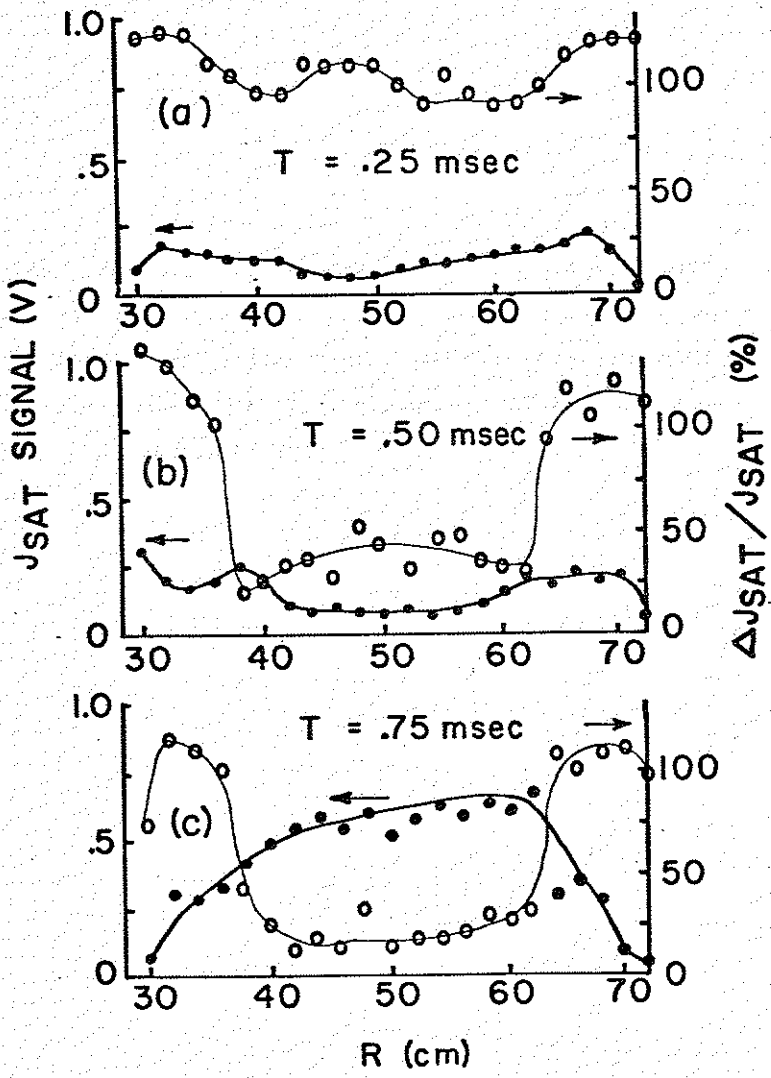

Figure 2-6.d,e,f) As a,b,c, but for later times. Note the expanded vertical scale in f, also the error bars on the fluctuations in f.

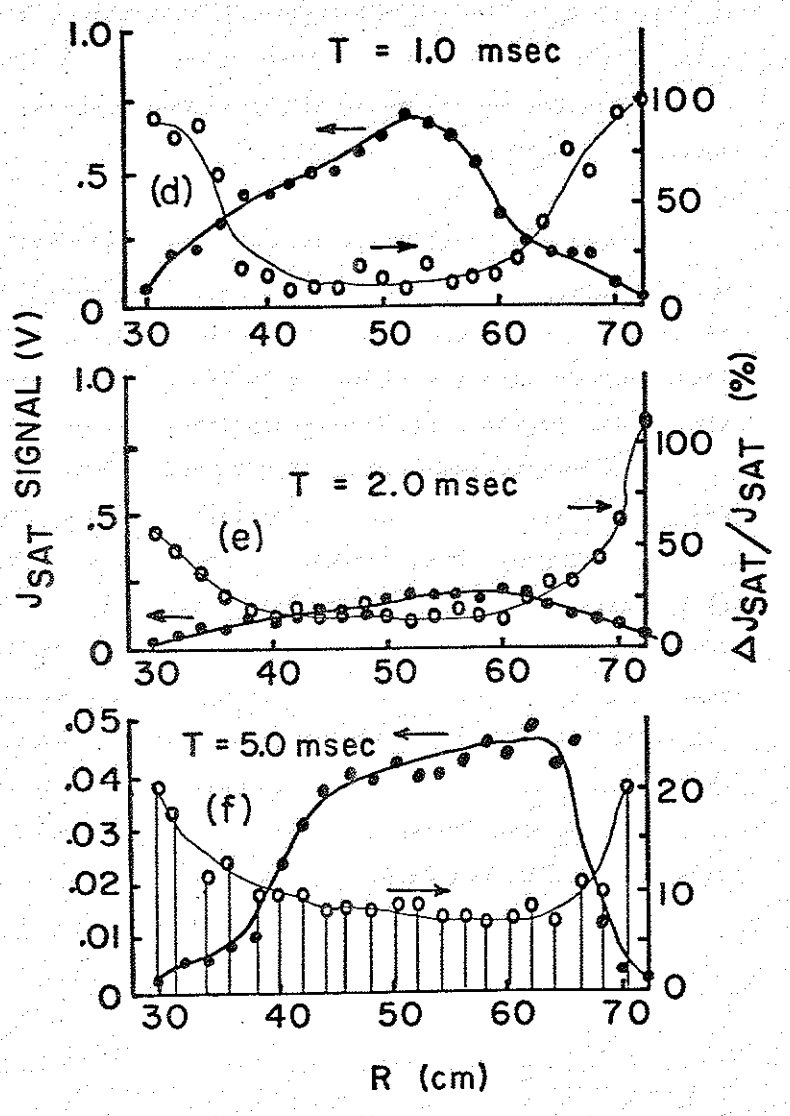

Figure 2-7. Radial T_e profile taken with small triple probe in midplane. The poloidal bank voltage is 2.0 kV.

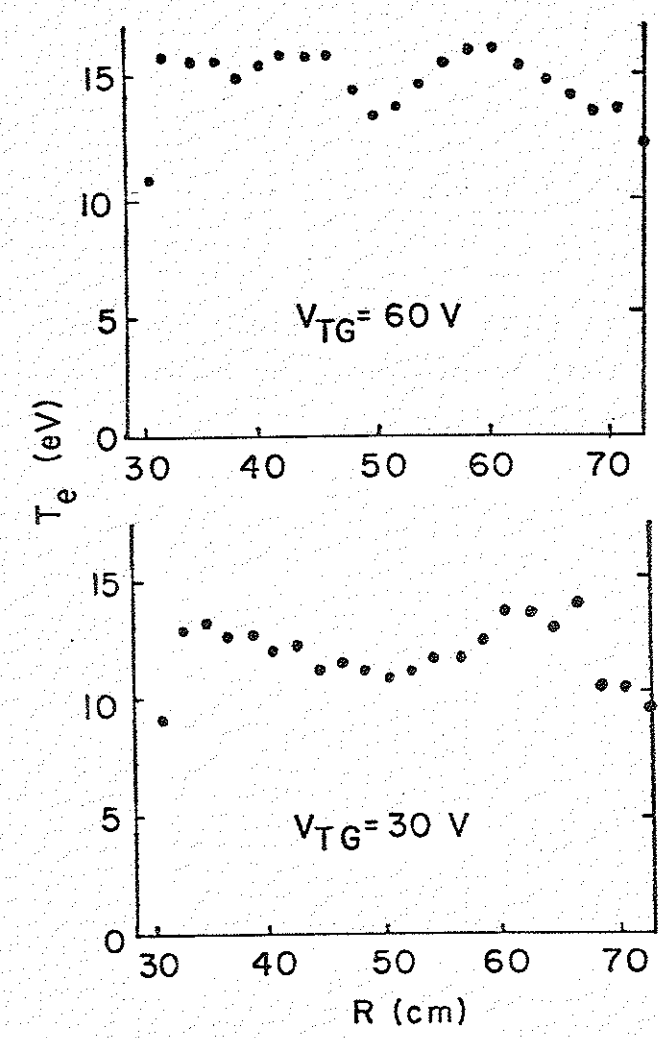

profile of T_e on the midplane made with a small triple probe; the temperatures shown here are in good agreement with those obtained from measurements of impurity radiation.

The poloidal current is strongly peaked at about Ψ = 7, as shown in Figure 2-8. Peak current densities of 10 A/cm^{-2} are typical in the midplane. The current rises roughly linearly with time until about 500 μsec after the heating voltage is applied, then decays to zero in about the same time. If the toroidal field is not crowbarred, so that the poloidal loop voltage reverses polarity as B_T decays, a second current peak of opposite sign to the first is seen toward the end of the B_T pulse. This second peak is always much smaller than the first peak and decays in typically $\lesssim$ 50 μsec after the poloidal loop voltage goes to 0. The spatial profile of the second peak is roughly the same as the first peak. Most of the measurements to be discussed were made during the first current peak.

Figure 2-8. Integrated $\Delta\dot{B}$ signal used to determine j_{pol} (dots) and j_{pol} profile derived from this signal (solid line). The difference between the heights of the two peaks is mainly due to the 1/R dependence of B_p.

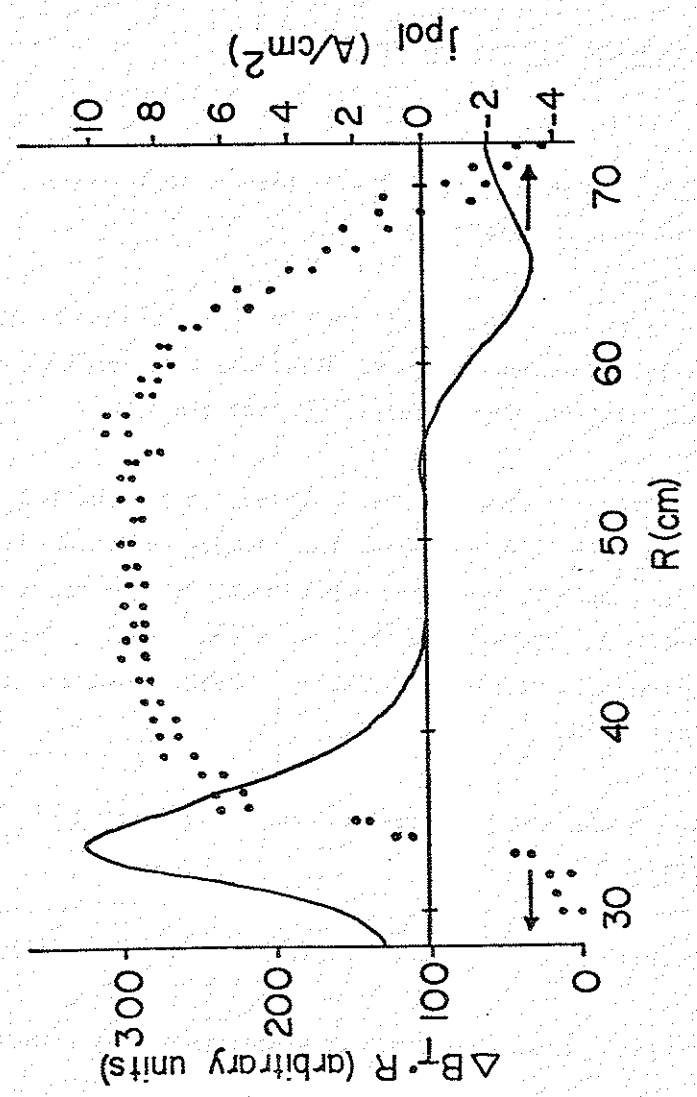

REFERENCES FOR CHAPTER TWO

1. J.C. Sprott and T.W. Lovell, University of Wisconsin PLP 744 (1978)

2. A.P. Biddle, R.N. Dexter, R.J. Groebner, D.J. Holly, B. Lipschultz, M.W. Phillips, S.C. Prager, and J.C. Sprott, Nucl. Fusion 19, 1509 (1979)

3. A.P. Biddle, R.N. Dexter, D.J. Holly, B. Lipschultz, T.H. Osborne, S.C. Prager, D.A. Shepard, J.C. Sprott, and P.D. Witherspoon, 8th International Conf. on Plasma Physics and Cont. Nucl. Fusion Research, Brussels, Belgium (1980), paper IAEA CN-32/X-4-1

4. L. Oren and R.J. Taylor, Nucl. Fusion 17, 1143 (1977)

5. H.F. Dylla, J. Nucl. Materials 93 & 94, 61 (1980)

6. R.A. Dory, University of Wisconsin PLP 15 (1966)

7. R.A. Dory, University of Wisconsin PLP 27 (1969)

8. The program is similar to the one described in D.A. Brouchous, Ph. D. thesis, University of Wisconsin (1980), Chapter V.

CHAPTER THREE: DIAGNOSTICS

A. MICROWAVE INTERFEROMETER

The phase shift that a beam of microwaves undergoes as it passes through a plasma can be used to measure the electron density. For the case of a cold collisionless unmagnetized plasma, the microwave radiation propagates with its wavelength increased from the vacuum value by the factor[1]

$$\mu = [1 - \frac{\omega_p^2}{\omega^2}]^{1/2}$$

where ω is the microwave frequency and $\omega_p = [\frac{ne^2}{m\epsilon_o}]^{1/2}$ is the plasma frequency. Thus the phase shift due to the plasma is

$$\Delta\phi = (1 - [1 - \frac{\omega_p^2}{\omega^2}])^{1/2} \frac{1}{\lambda_o} dx$$

where the integral is over the microwave propagation path and λ_o is the vacuum wavelength. For $\omega^2 >> \omega_p^2$ this becomes

$$\Delta\phi = \frac{e^2}{2m\epsilon_o\lambda_o}\int n_e \, dx$$

and thus the phase shift gives directly a line-averaged density over the microwave path.

In the presence of a magnetic field perpendicular to the microwave propagation the phase shift depends on the orientation of the radiation electric field with the magnetic field[2]:

$$\mu_{ext} = [\frac{(\omega^2-\omega_1^2)(\omega^2-\omega_2^2)}{\omega^2(\omega^2-\omega_{uh}^2)}]$$

where

$$\omega_1 = -[\frac{\omega_b}{2}] + ([\frac{\omega_b}{2}]^2 + \omega_p^2)^{1/2}$$

$$\omega_2 = +[\frac{\omega_b}{2}] + ([\frac{\omega_b}{2}]^2 + \omega_p^2)^{1/2}$$

$$\omega_{uh} = (\omega_b^2 + \omega_p^2)^{1/2}$$

$$\omega_b = \frac{e\,B}{m_e}$$

Interferometers of frequencies 40 GHz and 70 GHz have been used on Tokapole II to measure electron density. The beam passes through the midcylinder from top to bottom of the machine. Since Tokapole II is usually operated as a tokamak, with $B_T >> B_P$ on midcylinder, the interferometer horns are mounted with their E-plane parallel to B_T, so that primarily the ordinary mode is excited and the magnetic field does not affect the density measurements. However, in the poloidal heating mode, B_p is at least comparable to B_T on the midcylinder. The maximum magnetic field here is on the order of 3 kG; thus for an electron density of $n_e = 10^{13}$ cm-3, we have ω_b = 8.4 GHz, ω_p = 28 GHz, and μ_{ext} = .915. Neglecting the magnetic field leads to μ = .914. Thus the error in the density measurement

due to the magnetic field is .001/.086 = 1.1%, negligible in comparison to other errors. The corresponding values for the 40 GHz case are μ_{ext}=.680 and μ (neglecting B) = .704, which still leads to an error due to the magnetic field of less than 8%.

The 40 GHz interferometer system was constructed first, but was found to be cut off in normal (tokamak-like) discharges. Thus it was modified to the 70 GHz system shown in Figure 3-1. Most of the microwave "plumbing" was the Ka-band waveguide from the 40 GHz system, in order to reduce attenuation and save money. The klystron and detectors were mounted about a meter above the machine to reduce the effects of the toroidal field on the klystron. No special care was taken in the Ka-band bends for 70 GHz, yet they gave very little attenuation (<10%). The original 30° flare horn antennas were replaced with 8° flare horns in order to obtain adequate coupling.

In order to obtain density information from the interferometer, a zebra-stripe system[3,4] is used (Fig.3-2). The klystron frequency is modulated by a 1 μsec sawtooth wave, which is also fed to the y-axis of

Figure 3-1. 70 GHz interferometer system used to measure electron density on Tokapole II.

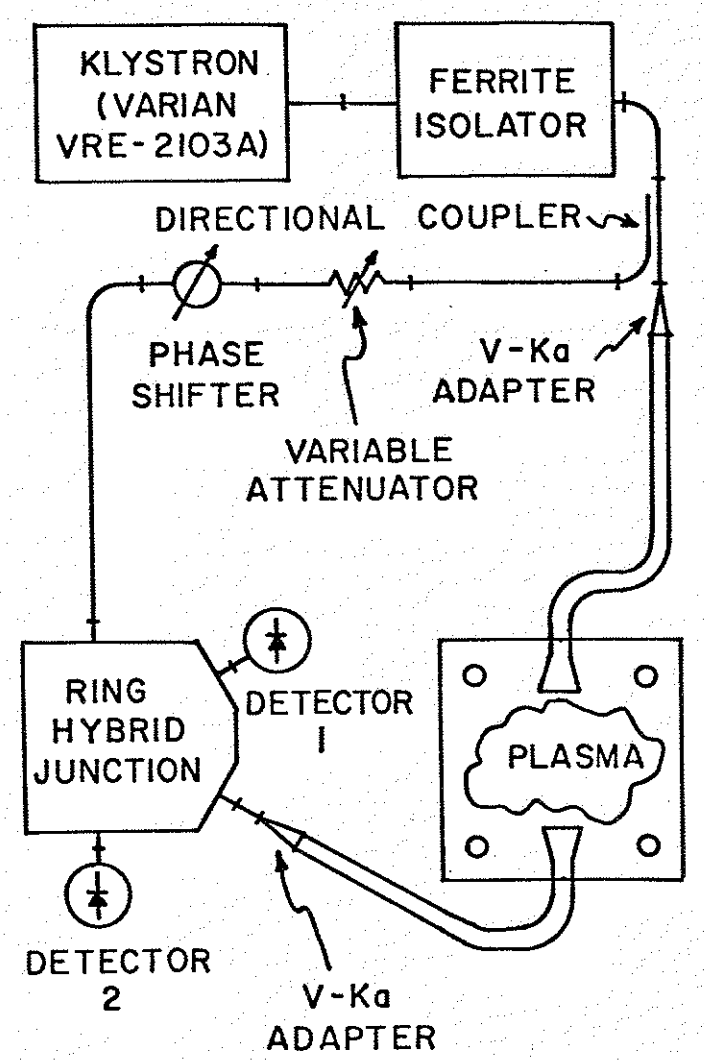

Figure 3-2. Zebra-stripe system used to extract electron density from interferometer of Figure 3-1.

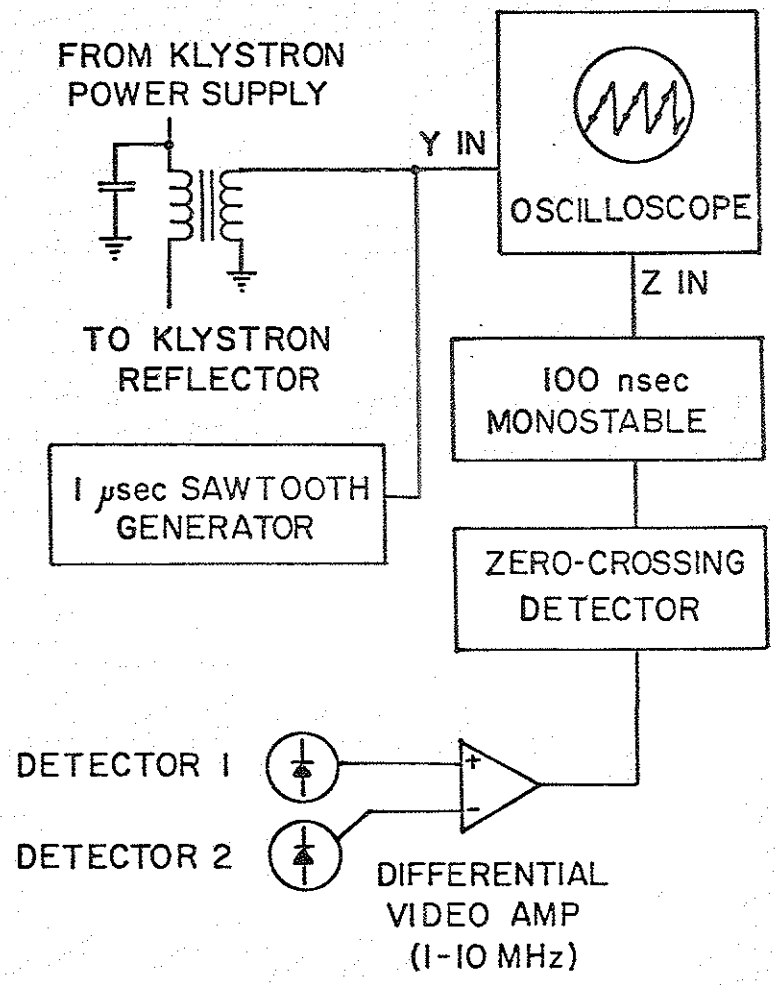

an oscilloscope. As the klystron's frequency varies, the zero-crossing detector senses interference minima due to the difference in electrical path length between the plasma arm and the reference arm of the interferometer, and unblanks the oscilloscope at the points where these minima occur. The plasma causes an additional phase shift in the plasma arm, causing the oscilloscope trace to be unblanked at a different point on the sawtooth sweep; the resulting display is a series of dots whose vertical displacement is directly proportional to the plasma-induced phase shift and thus to the line-averaged electron density. The sweep voltage is made large enough so that at least two interference minima occur per sweep, so that a trace is always visible on the oscilloscope. The system is absolutely calibrated in that the difference between two minima corresponds to one wavelength path length difference; thus if the plasma causes a vertical displacement corresponding to this, it means that the total electrical path length through the plasma has changed by one wavelength, which gives directly the change in line-averaged density.

Recently a digital circuit[5,6] which counts the fringes has been installed. This circuit gives an analog voltage which is directly proportional to the line-averaged density.

B. POLOIDAL CURRENT MEASURING TECHNIQUE

The poloidal plasma current can be measured by measuring the change it produces in the toroidal magnetic field. The toroidal field is the sum of the field due to the windings and the field due to the poloidal plasma current:

$$B_T = \frac{\mu_o}{2\pi R}(I_W + I_p)$$

$$= \frac{\mu_o}{2\pi R}(I_{W(VAC)} + \Delta I_W + I_p)$$

$$= B_{T(VAC)} + \Delta B_T$$

where I_W is the primary winding current, I_p is the poloidal plasma current, the subscript VAC indicates quantities in the absence of plasma, and Δ indicates the change due to the poloidal plasma current.

Since the probe responds to the net current flowing between it and the inside wall, the plasma current density profile can be obtained by making a radial scan of the plasma current:

$$j(R) = \frac{1}{2\pi R} \frac{\partial}{\partial R} I_R$$

where I_R is the net current between radius R and the major axis.

The probe consists of a 500-turn coil of fine copper wire about 1 cm long inside a 1/4-inch diameter tube of 15-mil stainless steel. The coil is wound on a G-10 form and is coated with non-corrosive RTV, and can be quickly replaced by pulling it from the stainless steel tube and soldering a new coil in its place. The probe's frequency response is flat up to about 300 kHz. The probe is inserted through a port into the major axis on the midplane and oriented as in Figure 3-3, so that the probe output is proportional to $\dot{B}_T$.

The circuit of Figure 3-4 is used to extract the poloidal current from the $\dot{B}_T$ measurement. The plasma current signal is only a few percent of the winding

Figure 3-3. $\dot{B}$ probe used to measure poloidal plasma current by measuring the change produced in the toroidal field.

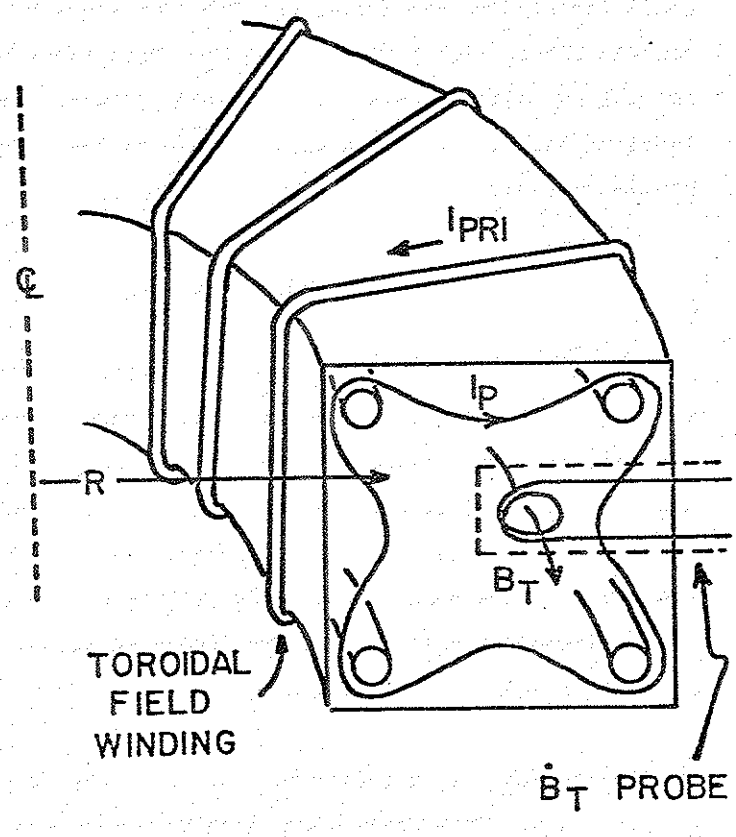

Figure 3-4. Circuit used to extract poloidal plasma current from measurement of $\dot{B}_T$.

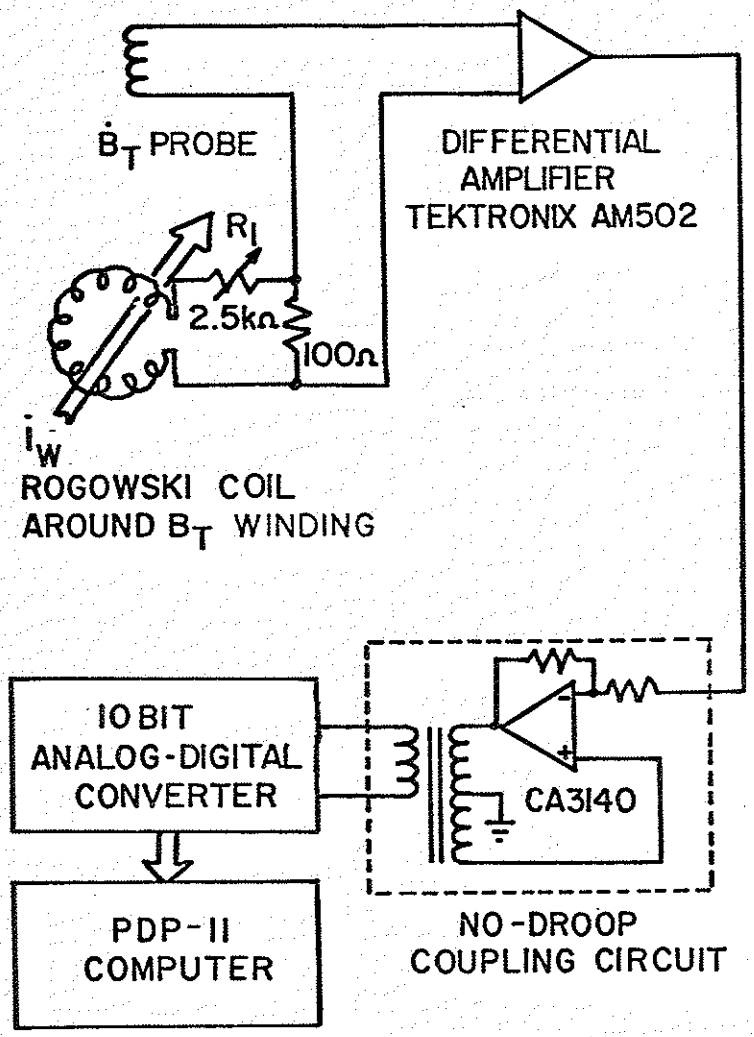

signal upon which it is superimposed, so it is not trivial to accurately separate the plasma current signal. First the fields are fired without puffing any gas, so that no plasma is produced, and R_1 is adjusted until the winding current signal from the Rogowski coil cancels the $\dot{B}_T$ signal from the probe. Then the machine is pulsed with plasma; the nulled signal, after integration, is directly proportional to the poloidal plasma current:

$$I_p = \frac{2\pi R}{\mu_o} \Delta B_T - \Delta I_W$$

In practice the nulling is not perfect so the computer must take a no-plasma baseline for each shot and subtract it. This leads to an error of $\epsilon \Delta I_W$ in the measured plasma current, where ϵ is the ratio of the nulled signal to the un-nulled signal. Since ϵ is typically a few percent and since ΔI_W is on the order of I_p, imperfect nulling leads to errors of only a few percent in measuring the plasma current.

A typical I_p waveform obtained this way is shown in Fig. 3-5. To prevent droop problems the coupling circuit[6] shown schematically in Figure 3-4, rather than

Figure 3-5. Typical poloidal plasma current vs. time obtained as shown in Figure 3-4.

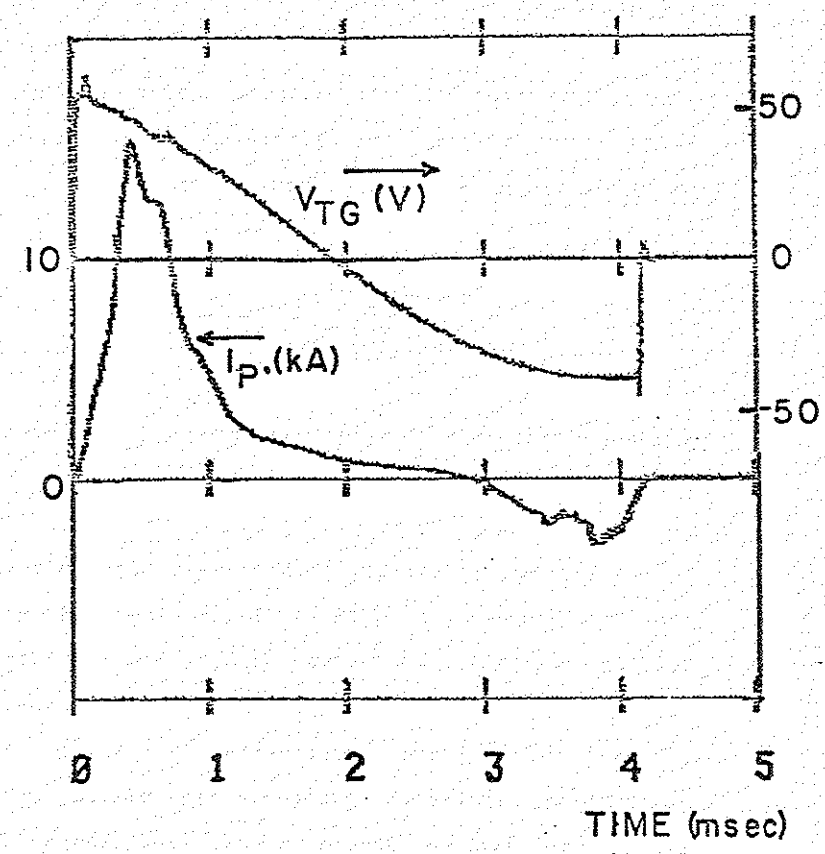

a simple transformer, is used to isolate the signal path to the computer. Also, the signal integration is done by the computer, to minimize noise pickup and droop. The circuit is calibrated by measuring the un-nulled vacuum B_T signal; then

$$\frac{B_T - \frac{\mu_o}{2\pi R}\Delta I_W}{B_{T(VAC)}} = \frac{I_P}{I_{W(VAC)}}$$

and since the winding current is known, the poloidal plasma current is determined absolutely.

A few current density measurements were made using other techniques. A small (~1 cm inner diameter) movable Rogowski coil[8] was used to measure both the toroidal and poloidal components of I_P; however, because this probe represents a fairly large obstruction, because it requires a high plasma current density to give a usable signal, and because it is sensitive to magnetic field pickup unless it is very carefully wound and the field is uniform in space, it could not be used except at the highest current densities. For low current density measurements, a

paddle probe[9,10] was used; however, the poor saturation of electron current with bias voltage, especially at high electron densities, and probe surface effects, make this probe suitable only at low electron densities. Even at low densities the accuracy of paddle probe measurements is poor. The advantage of these two alternate techniques is that they measure a truly local current density and can measure both poloidal and toroidal currents; the $\dot{B}_T$ technique can measure only the toroidal average of the poloidal current density, but generally with good accuracy.

C. LANGMUIR PROBES

Langmuir probes were used to obtain local measurements of electron density, electron temperature, and floating potential. Since discussions of elementary Langmuir probe theory are widely available elsewhere[11,12], this section will be limited to a brief description of their use in these experiments.

Local electron density was measured using single- or double-tipped Langmuir probes biased to collect ion saturation current. The probe body consisted of a 1/4-inch o.d. stainless steel tube ending in a ceramic rod through which the small (.Ø5 inch diameter x .1 inch long) platinum wire probe tips protuded. The probe is biased to about -75 V. Usually a double probe[13] was used to minimize errors due to floating potential fluctuations;[9] in this mode both tips are left floating and the voltage across the current-measuring resistor is monitored via a differential amplifier.

In addition to these localized density measurements, a line-averaged density was obtained using a fixed Langmuir probe. This was located between an outer ring and the wall and was specially shaped so as to correctly volume-weight the flux surfaces[14]. This probe was calibrated against the microwave interferometer and found to agree well in the poloidal-ohmically-heated discharges (Figure 3-6). The movable Langmuir probes were also calibrated against the interferometer.

Figure 3-6. Density measurements during a poloidal ohmic heating shot made with zebra-stripe interferometer (top trace in a,b,c) and with line-averaged Langmuir probe (bottom trace in a,b,c). The horizontal scale is a) Ø.2 msec/division, b) Ø.5 msec/division, and c) 1 msec/division. The distance between interferometer stripes represents a density change of 1.2×10^{12} cm^{-3}. The line-average probe scale is roughly 1.1×10^{12} cm^{-3} (assuming $T_e \sim 10$ eV).

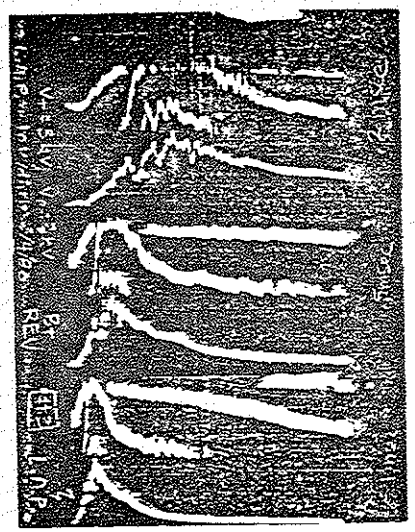

Electron temperature can be obtained by sweeping a Langmuir probe or with a triple-tipped Langmuir probe.[13,15] Both methods were used to obtain T_e profiles and gave similar results, although both gave large (~50%) uncertainties in T_e. The triple-probe method was also used with 3 fixed probes located on the separatrix to obtain electron temperatures during scaling and resistivity measurements. These electron temperatures are comparable to those obtained from impurity radiation measurements as described in the next section.

D. IMPURITY RADIATION DETECTORS

In most of the plasmas studied using poloidal ohmic heating in Tokapole II, the hydrogen is fully ionized in most regions of the discharge and cannot emit line radiation. Most of the electromagnetic radiation produced by the plasma is line radiation from partially stripped impurity ions. This impurity radiation can be used to measure the plasma's electron temperature.

Groebner[16,17] developed a computer code which determines the time evolution of electron temperature in standard Tokapole II discharges from measured ratios of oxygen radiation lines, based upon a time-dependent coronal model. This code is used to determine peak electron temperatures in poloidal ohmic discharges. The code solves a set of rate equations for the densities of the various ionization levels of oxygen of the following form:

$$\frac{dn_o}{dt} = -S_o(T_e)n_e n_o + \alpha_1(T_e)n_e n_1 - \frac{n_o}{\tau} + \Phi_o$$

$$\frac{dn_z}{dt} = -S_z(T_e)n_e n_z - \alpha_z(T_e)n_e n_z + S_{z-1}(T_e)n_e n_{z-1}$$

$$+ \alpha_{z+1}(T_e)n_e n_{z+1} - \frac{n_z}{\tau}$$

$$\frac{dn_{z+1}}{dt} = -\alpha_{zL}(T_e)n_e n_{zL} + S_{zL-1}(T_e)n_{zL-1}n_e - \frac{n_{zL}}{\tau}$$

where n_z is the density of oxygen ions of charge z, n_e is the electron density, τ is the particle confinement time, Φ_o is the influx rate of atomic oxygen, and zL refers to the most highly charged oxygen ion produced

by the plasma. S_z is the ionization rate coefficient for an ion with charge z and α_z is the recombination rate for ion z going to z-1. The calculation is zero-dimensional. The electron density used is obtained experimentally from microwave interferometer measurements; τ and Φ_o must also be estimated from experimental data, although the results of the code are quite insensitive to their values. A guess is made of the electron temperature as a function of time, and this is used as another input to the code; the code gives as output intensities of oxygen line radiation as a function of time, and the input electron temperature is varied until the radiation intensities match the experimental data.

Oxygen impurity lines which give usable intensities in poloidal ohmic discharges are in the vacuum ultraviolet and range from those of O I (neutral oxygen, which has an ionization energy of 13.6 eV) to O VI (oxygen with five electrons removed, which has an ionization energy of 138 eV). The experimental line intensities all peak at very nearly the same time, so that the code gives little information about the time dependence of T_e, but does give a peak T_e.

Groebner estimates that the technique gives T_e accurate to about 50%. The results obtained in poloidal ohmic discharges on Tokapole II agree well with results from triple Langmuir probes and swept Langmuir probes. The validity of the time-dependent coronal equilibrium code method is further supported by T_e measurements made on the Wisconsin Levitated Octupole with admittance probes and using ratios of carbon lines from the same ionization state; both methods give excellent agreement with the code results.

In addition to its use as a T_e diagnostic, impurity radiation is potentially important as an energy loss mechanism. A 1/2-m Seya monochromator with a Channeltron array in place of its exit slit is used to monitor the total vacuum ultraviolet radiation on Tokapole II. The total current to the Channeltron array is proportional to the VUV radiation integrated over wavelengths from about 500 Å to 1300 Å. The signal from this monitor is always much less during poloidal ohmic discharges than during standard Tokapole II discharges, despite the fact that up to 2 MW of power is coupled into the plasma by poloidal ohmic heating, compared to the several hundred kW in a

standard discharge. Since only a small fraction of the input power in a standard discharge is lost through impurity radiation,[18] clearly impurity radiation is not an important loss mechanism for poloidal ohmic heating.

REFERENCES FOR CHAPTER THREE

1. F.F. Chen, Introduction to Plasma Physics (Plenum Press, New York, 1974)

2. J. Farrand, University of Wisconsin PLP 224, (1968)

3. M.A. Heald and C.B. Wharton, Plasma Diagnostics with Microwaves (John Wiley and Sons Inc., New York), 1965

4. T. Kruzel, University of Wisconsin PLP 831 (1980)

5. C.M. Fortgang, University of Wisconsin PLP 861 (1981)

6. H.R. Garner, University of Wisconsin PLP 833 (1981)

7. Don Holly and Tom Lovell, "Op Amp Reduces Transformer Droop", EDN, October 5, 1979

8. G. Barney and J. Hawxhurst, University of Wisconsin PLP 38 (1974)

9. D.E. Lencioni, University of Wisconsin PLP 286 (1969)

10. J.F. Etzweiler, University of Wisconsin PLP 619 (1975)

11. F.F. Chen, Plasma Diagnostic Techniques (R.H. Huddlestone and S.L. Leonard, eds., Academic Press, New York, 1965), Chapter 4

12. J.C. Sprott, University of Wisconsin PLP 88 (1966)

13. J.C. Sprott, University of Wisconsin PLP 109 (1967)

14. The probe is similar to the one described in E.J. Strait, University of Wisconsin PLP 566 (1974)

15. S. Chen and T. Sekiguchi, J. Appl. Phys. 36, 2363 (1965)

16. R. Groebner, J.C. Sprott, R.N. Dexter, University of Wisconsin PLP 796 (1980)

17. R. Groebner, Ph.D. Thesis, University of Wisconsin (1980)

18. R.J. Groebner and R.N. Dexter, Plasma Physics 23, 693 (1981)

CHAPTER FOUR: RESISTIVITY THEORY AND MEASUREMENT

A. SPITZER RESISTIVITY

In the presence of an electric field, electrons in a plasma accelerate until they undergo collisions which convert the directed energy they acquire from the electric field to randomly-directed thermal energy. This gives rise to a resistivity[1]

$$\eta = \frac{m\nu}{n e^2}$$

where m is the electron mass, n the density of current-carrying electrons, and ν is the collision frequency. For a fully ionized, unmagnetized plasma, the dominant collision frequency is ν_{ei}, the effective frequency at which electrons collide with ions changing the electrons' velocities by 90°. Only the electron-ion collisions are involved, since electrons

carry most of the current and electron-electron collisions produce no net change in the electrons' momentum. However, electron-electron collisions do play a part in that they modify the electron velocity distribution, which in turn affects ν_{ei}. Assuming Z = 1 and including electron-electron collisions, Spitzer[2] derives

$$\eta = 6.53 \times 10^{-3} \frac{\ln \Lambda}{T_e^{3/2}} \quad \Omega\text{-cm}$$

where T_e is in eV and $\ln \Lambda$ is the Coulomb logarithm

$$\Lambda = \frac{\lambda_D m v_e^2}{Ze^2}$$

Here λ_D is the Debye length and v_e is the electron thermal speed. $\ln \Lambda$ is about 10 for the plasmas studied here.

If mechanisms other than electron-ion collisions are available to randomize the electrons' momentum, the effective collision frequency ν increases from ν_{ei}, and the resistivity is enhanced above the Spitzer value.

B. MIRROR TRAPPING AND COLLISIONALITY

In the presence of a magnetic field which varies in space, some of the electrons are trapped in the magnetic wells and are unable to respond to an electric field parallel to the magnetic field. The effect on the resistivity[3,4,5] varies with the relative magnitudes of ν_{ei}, ν_b, and ν_{lc}. Here ν_b is the bounce frequency for trapped electrons, the electrons' thermal speed divided by the mirror length:

$$\nu_b = \frac{v_{e\ th}}{L_m}$$

L_m is defined as half the distance along field lines

between magnetic field maxima. ν_{lc} is the frequency at which electrons are scattered by small-angle collisions out of the mirror loss cones in velocity space and become trapped in the magnetic mirrors. If this scattering is due to electron-ion collisions, a random walk in velocity space leads to[3]

$$\nu_{lc} = \left(\frac{\pi/2}{\theta_{lc}}\right)^2 \nu_{ei}$$

with

$$\sin^2 \theta_{lc} = \frac{B_{min}}{B_{max}} = 1/M$$

Depending on the relative magnitudes of these three collision frequencies, there are three collisionality regimes:

a. Highly collisional: $\nu_{ei} >> \nu_b$

Here an electron undergoes many electron-ion collisons in the time it would take to bounce in the magnetic mirror. Thus the electron is never really trapped by the mirror, and the electron-ion collision frequency alone determines the resistivity:

$$\eta = \frac{m \nu_{ei}}{ne^2} = \eta_{Sp}$$

b. Highly collisionless: $\nu_{ei} << \nu_b$

Here the electrons are trapped at a rate ν_{lc} and then bounce in the mirrors many times before they are de-trapped by a collision. The mirror-trapped electrons cannot contribute to the current, so that the density of current-carrying electrons is reduced from n_e to a fraction $f_{ut} n_e$, where f_{ut} is the fraction of electrons which are untrapped by the mirrors. Ignoring the imposed electric field, for an isotropic electron distribution f_{ut} depends only on the mirror ratio; the

presence of a strong electric field modifies this by giving some of the trapped electrons enough parallel velocity to overcome the magnetic well. This leads to[6]

$$f_{ut} = 1 - \sqrt{1 - 1/M} \quad \exp\left(\frac{-eE_{\parallel}}{M-1} L_{bounce}/kT_e\right)$$

where L_{bounce} is the total distance along field lines between field maxima and $E_{\parallel}$ is the magnitude of the electric field parallel to the magnetic field.

Since the electrons are removed from the circulating region of velocity space at a rate ν_{1c}, the resistivity is

$$\eta = \frac{m \nu_{1c}}{f_{ut}\, n\, e^2} = \left(\frac{\pi/2}{\theta_{1c}}\right)^2 \frac{m\nu_{ei}}{e^2 f_{ut}\, n}$$

$$= \left(\frac{\pi/2}{\theta_{1c}}\right)^2 \frac{\eta_{Sp}}{f_{ut}}$$

Thus in the highly collisionless regime the resistivity scales as Spitzer resistivity, but is enhanced by a factor which depends mainly on the mirror ratio.

c. Intermediate Regime: $\nu_{ei} < \nu_b < \nu_{1c}$

Here the electrons are removed by small-angle collisions from the circulating region of velocity space at a rate ν_{1c}, but after they are "trapped", they do not bounce in the mirrors until a relatively long time later $t \sim 1/\nu_b$. Thus they must be considered as contributing to the current during this time, and the effective frequency at which they are removed from the circulating electrons is ν_b. Again only a fraction f_{ut} of the electrons carries the current, so that the resistivity in the intermediate regime is

$$\eta = \frac{m\nu_b}{e^2 f_{ut}\, n_e} = \frac{m\, v_e}{e^2 L_m f_{ut}\, n_e}$$

Note that the effective mean free path here is $L_m\ f_{ut}$, which depends mainly on machine parameters, and only very weakly on the electron temperature. Because of this independence of the mean free path from plasma parameters the intermediate collisionality regime is often referred to as the plateau regime.

C. OTHER RESISTIVITY EFFECTS

Besides the effects of mirror trapping, other phenomena which can modify the plasma resistivity from the value calculated by Spitzer include collisions with neutrals, runaway electron effects, and interactions with fluctuations.

If the current-carrying electrons encounter so many neutral atoms or molecules that the electron-neutral collision frequency ν_{en} becomes comparable to ν_{ei}, then ν_{en} becomes an important factor in determining the resistivity. Scattering from neutrals is different from electron-ion scattering in that it does not involve the long-range Coulomb force; thus the electrons which scatter from neutrals are

those with small impact parameters, and the scattering angle is typically large. Thus if neutral collisions dominate ion collisions, one cannot simply replace ν_{ei} by ν_{en} in the mirror resistivity expressions of the previous section.[4] In the poloidal ohmic heated discharges, however, neutrals usually play only a small part in the resistivity, so that simple approximations for their effect are adequate. Smith,[7] using cross-section data obtained from Gilardini,[8] gives analytic expressions for ν_{en} for molecular hydrogen:

$$\nu_{en} = 1.05 \times 10^{-7}\, n_{H_2}\, (T_e^{.7} + .0114),\quad T_e < 1 \text{ eV}$$

$$= 1.04 \times 10^{-7}\, n_{H_2}\, (T_e^{.3} + .0246),\quad 1 \text{ eV} < T_e < 10 \text{ eV}$$

$$= 2.10 \times 10^{-7}\, n_{H_2},\quad T_e > 10 \text{ eV}$$

where ν_{en} is in $\sec^{-1}$, T_e is in eV, and n_{H_2} is in cm^{-3}. All of the poloidal ohmic heating data falls in the latter two temperature regimes. The electron-ion collision frequency used in calculating Spitzer resistivity is[9]

$$\nu_{ei} = 1.5 \times 10^{-6} \frac{n_e \ln \Lambda}{T_e^{3/2}}$$

with n_e in cm^{-3} and T_e in eV. For most of the poloidal ohmic heating cases the plasma is believed to be strongly ionized and $\nu_{ei} >> \nu_{en}$ as determined from these expressions; but for the cases in the low collisionality regime, collisions with neutrals can be significant. Frost[10] and Johnson[11] have done more careful calculations of the effect of ν_{en} on the resistivity, but Etzweiler[4] has shown that simply adding the ion-dominated resistivity to the neutral-dominated resistivity, $\eta = \eta_{Sp} + \eta_{neutral}$, leads to errors no greater than about 25%. Thus in the cases where neutrals have a significant effect on the resistivity, we have simply added the two terms as resistors in series.

Runaway electrons are produced when the applied electric fields are so high that electrons gain more energy between collisions than the collisions dissipate. This is possible because the cross section

for electron-ion collisions decreases as the electron velocity increases. Dreicer[12] calculated the critical electric field above which electrons can run away:

$$E_c = \frac{\nu_{ei}\, m\, v_{e\ th}}{e}$$

$$= 10^{-10} \frac{n_e}{T_e} \text{ V/m}$$

with n_e in cm^{-3} and T_e in eV. Furthermore, he pointed out[13] that even below this field, electrons in the high-energy "tail" of the distribution can run away, distorting the electron energy distribution and possibly providing a source of energy to drive instabilities.

A parameter which is closely related to E/E_c and which is also used to determine the theoretical threshold of instabilities is the ratio of electron streaming speed to electron thermal speed, $v_d/v_{e\ th} = j/f_{ut} n e v_{e\ th}$. Note that for $\eta = \eta_{Sp} = m\nu_{ei}/ne^2$, the two expressions $v_d/v_{e\ th}$ and E/E_c are identical.

Buneman[14] considers the coupling of energy from runaway electrons into a two-stream instability and obtains the result that within a time on the order of a hundred plasma periods ($100 \times 2\pi/\omega_{pe}$) the drifting energy of the electrons should be coupled into instabilities. From this he derives a turbulent resistivity for $E > E_c$:

$$\eta_{Buneman} = (200\pi\epsilon_o\omega_{pe})^{-1}$$

Demidov[21] derived a turbulent resistivity

$$\eta_{Demidov} = 2 \times 10^7 \frac{T_e^{1/2}}{(n_e r)} \Omega\text{-m}$$

where r is the distance in meters to the wall, n_e is in cm^{-3} and T_e is in eV. He assumed that the two-stream instability took energy from the drifting electrons and that this energy was then absorbed primarily by the

machine wall, rather than by the plasma. His experimental turbulent heating data were in good agreement with this resistivity; furthermore, he observed microwave emission from the plasma at $\sim\omega_{pe}$, as expected from the two-stream instability.

Even when the electric field is well below E_c, the streaming energy of the electrons may excite instabilities which increase the resistivity above η_{Sp}. Coppi and Mazzucato[15] consider the effect of drift waves on resistivity and find resistivity enhancement commencing at E/E_c ratios as low as 10^{-2}. The instabilities onset[16] when the electron streaming velocity is roughly equal to or exceeds the ion sound velocity $c_s = (kT_e/m_i)^{1/2}$. Smith and Hollweg[17] calculate threshold streaming velocities for a variety of current-driven instabilities; in general, for $T_i \ll T_e$ the instabilities are excited at electric fields well below the Dreicer critical field.

For applied electric fields not much greater than E_c, the ion-acoustic instability should provide sufficient resistivity to keep $v_d \sim v_{e\,th}$.[18] If $E \gg E_c$, the streaming velocity can increase above $v_{e\,th}$ and

stronger turbulence at frequencies much higher than ion-sound instability frequencies can occur, giving a turbulent resistivity $\propto \omega_{pe}^{-1}$. If this turbulence again slows down the drifting electrons, the ion-sound instability may again dominate the resistivity.[19]

D. PREVIOUS RESISTIVITY MEASUREMENTS

The first experimental studies of resistivity in a toroidal octupole were done by Lencioni[3,20], using a gun-produced plasma with $n_e \sim 10^9$ cm^{-3} and $T_e \sim 10$ eV. He used paddle probes to measure current densities near the minor axis for electric fields $E_\parallel$ up to about 10 V/m (far in excess of the Dreicer critical field). Lencioni found that below the point where the induced current density j was about half of the thermal current, the current was proportional to $E_\parallel$; above this point it saturated. For $E_\parallel \lesssim 5$ V/m, he obtained

$$\eta = 2.5 \times 10^7 \frac{\sqrt{T_e \text{ (eV)}}}{n \text{ (cm}^{-3})} \Omega\text{-m}$$

This was too high to be explained by either the collisionless mirror-limited Spitzer resistivity of section B or by Buneman's turbulent conductivity. The result indicates a constant electron mean free path in the low collisionality regime, as if the plateau regime scaling continued where the collisionless scaling was expected. The resistivity was in rough agreement with the result derived by Demidov[21] in scaling like $\sqrt{T_e}/n\,r$, although the magnitude was about a factor of four less than Demidov's result.

Guss[22] measured resistivity in a small toroidal quadrupole and obtained, for some operating modes, roughly the same form for the conductivity as Lencioni, although the quadrupole electric field $E_\parallel$ was less than the Dreicer critical field. The magnitude of the resistivity was about a factor of 5 less than Demidov's result, but approximately the same as mirror-limited Spitzer resistivity.

Etzweiler[4] extended the resistivity measurements in the small Wisconsin Octupole by ohmically heating an ECRH microwave-produced plasma to give densities up to several times 10^{12} cm^{-3} with electron temperatures T_e

~5 to 20 eV. Brouchous[3,5] studied resistivity in the Wisconsin Levitated Octupole using plasma produced by each of three different coaxial guns. This allowed him to vary n_e from 10^9 cm^{-3} to 10^{12} cm^{-3}, with T_e ranging from ~2 eV to ~10 eV. Between the two experiments, all three collisionality regimes were accessible. At high and intermediate collisionalities the resistivity followed the predictions of section B, but at low collisionality the resistivity continued to follow the intermediate regime scaling. The variation of resistivity seen by Brouchous and Etzweiler is summarized in Figure 4-1. Brouchous was able to eliminate the ring supports as a possible cause for the anomalous resistivity at low collisionality by levitating the rings: the supports could be withdrawn for 20 msec by a pneumatic mechanism while the rings remained in position due to their inertia. Withdrawing the supports did not affect the anomalous resistivity. Brouchous and Etzweiler believed scattering from current-driven fluctuations was responsible for the anomalously high resistivity in the collisionless regime.

Figure 4-1. Variation of resistivity with collisionality observed by Brouchous and Etzweiler (reference 5). The two lines shown labeled "small octupole" represent the limits of the plateau regime mirror scaling for the electric fields used by Etzweiler; the electric fields on the large octupole are so small that the theory is represented by a single line, labeled "large octupole". The horizontal scale is equivalent to ν_b/ν_{ei}. Crossover from the Spitzer to the intermediate regime is shown at $\nu_b/f_{ut} = \nu_{ei}$; crossover from the intermediate to the collisionless regime is at $\nu_b = \nu_{lc}$.

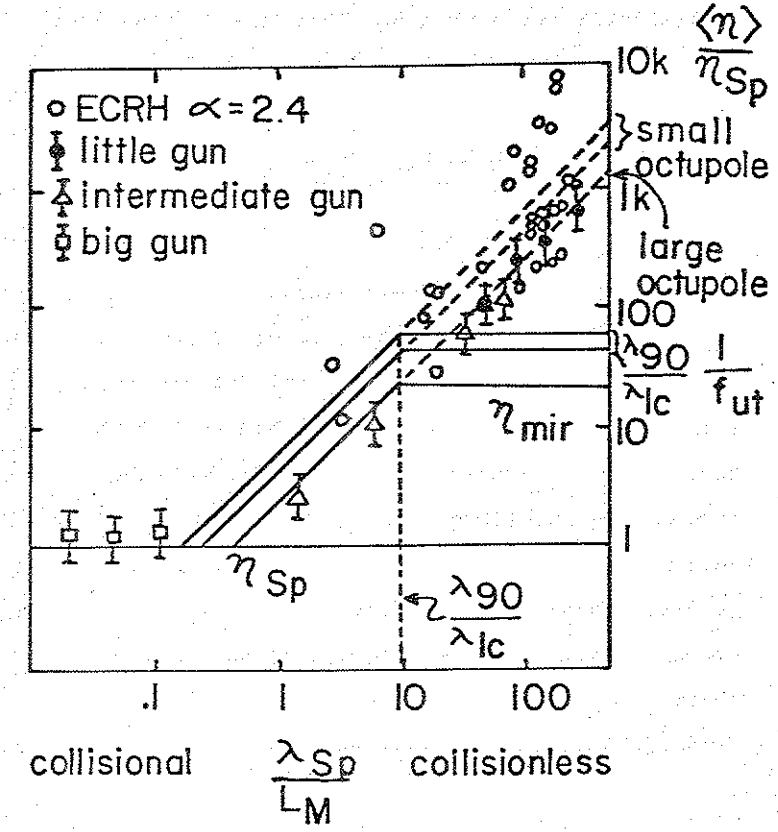

A number of other experiments have studied the effects of fluctuations and turbulence on plasma resistivity. Hamberger[23] at Culham, using a small stellarator, applied electric fields ranging from 10^{-1} V/cm to 10^{3} V/cm to turbulently heat a plasma with initial density ranging from 10^{10} cm^{-3} to 10^{13} cm^{-3}. A similar experiment was performed by Demidov et al[24] with similar results. The resistivity as a function of applied field exhibited three plateau regions with sharp jumps between the regions. Hamberger believed that the jumps in resistivity corresponded to the onset of the ion-sound wave and the two-stream instability respectively. The $(M/m)^{1/3}$ ω_{pe}^{-1} dependence predicted by Buneman for the regime with $E >> E_c$ was also verified by changing the gas used and varying the density. In both experiments the magnetic field simply provided containment for the initial plasma and did not affect the resistivity. Hamberger also measured fluctuation frequencies and found them in agreement with the ion-sound instability and the two-stream instability in the corresponding electric field regimes.[25]

More recent experiments[18,26] on the Texas Turbulent Torus, a device built to test turbulent heating, found resistivities of the same magnitudes as those of Hamberger and Demidov, but found the resistivity to vary as roughly the square root of the applied electric field. Enhanced outward transport was also seen, while the hoped-for rapid skin penetration was not observed: the skin time was as expected from the resistivity measurements.

Recent resistivity data taken by Brouchous[27] on the Levitated Octupole strongly support the fluctuation explanation of the anomalous resistivity. In these experiments, the plasma was observed to undergo a quiet phase in its decay, with density fluctuations $\delta n/n < 2\%$. Brouchous measured the resistivity during this quiet phase, and found that the measurements at low collisionality fell on the mirror-limited Spitzer line, rather than continuing to rise as in previous experiments. Resistivity measurements taken during the noisy period of the same shots continued to follow plateau scaling at low collisionalities, as previous measurements had done. Thus there is good reason to

associate the high resistivity usually seen at low collisionalities with scattering from fluctuations.

E. METHOD OF DETERMINING RESISTIVITY

In order to find the plasma resistivity for current flow along field lines, three things must be measured or calculated: the electric field, the current density, and the geometric effects of the magnetic field structure. The electric field is calculated as described in section 2-D; since the poloidal field is crowbarred, the electric field is assumed to be purely poloidal, and since the plasma current is small (a few percent) compared to the winding current, the vacuum electric field is used in calculating resistivity. The local poloidal current density is measured with a $\dot{B}$ probe as described in section 3-B.

To include the effect of the magnetic field shape,[28] the resistivity must be averaged so as to take into account the varying cross-sectional area through which the current flows as it follows the magnetic

field lines. The resistance of the region between two poloidal flux surfaces once around poloidally is

$$R(\Delta\Psi) = V_{\parallel} / I(\Delta\Psi) = \int (\eta / A_{\perp}) \, dx$$

where $V_{\parallel}$ is the poloidal voltage once around poloidally at Ψ and $I(\Delta\Psi)$ is the total current flowing parallel to the field lines between the two surfaces. dx is an element of length measured parallel to the total field and $A_{\perp}$ is the total area perpendicular to B through which the current flows.

By the definition of Ψ, the surface between two flux surfaces perpendicular to the poloidal field (shown as the annulus A in Figure 4-2) has area $(\Delta\Psi/B_p)$. If the current flows around twice poloidally as it makes one toroidal revolution, then the area perpendicular to B_p through which the current flows is A/2; or in general

$$A_{\perp} B_p = A^* q = q \, (\Delta\Psi/B_p)$$

Figure 4-2. Annulus A formed by the intersection of the midplane with two poloidal flux surfaces.

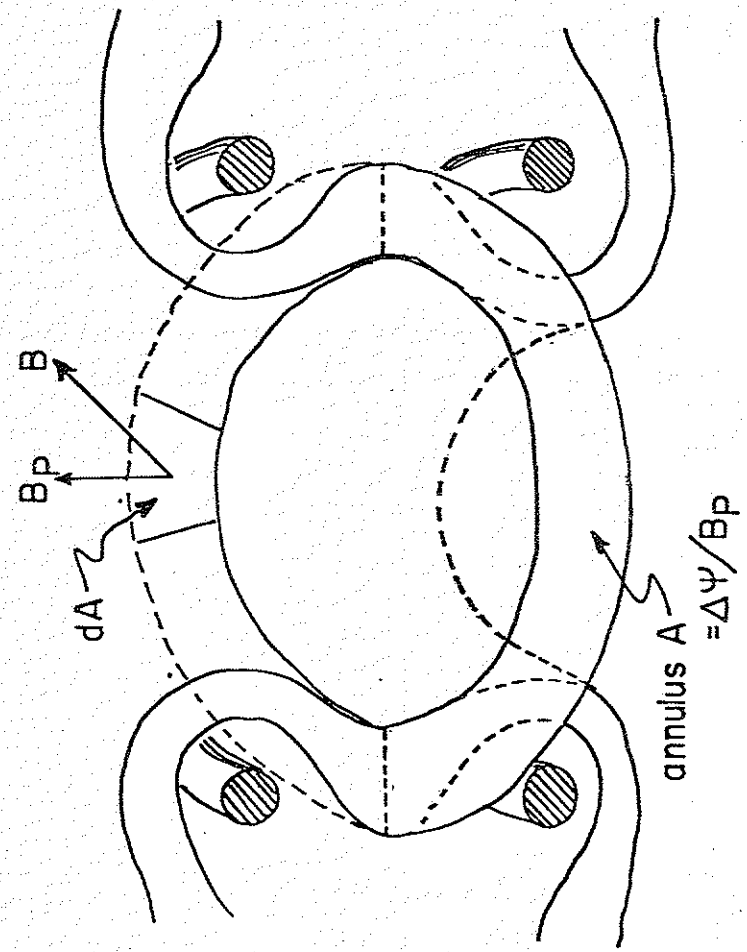

where q is the safety factor. The projection of this area perpendicular to the total field B is $A_\perp$:

$$A_\perp = q\,(\Delta\Psi/B_p)\,(B_p/B)$$

and since $dl = (B_p/B)\,dx$, where dl is an element of length measured parallel to the poloidal field,

$$R(\Delta\Psi) = \int \eta (B/(B_p \times A_\perp))\,dl = \int \frac{\eta B^2}{B_p\, q\, \Delta\Psi}\,dl$$

q and $\Delta\Psi$ are independent of the location along the flux surface. If η is also constant on a flux surface,

$$R(\Delta\Psi) = V_\parallel / I(\Delta\Psi) = \frac{\eta}{q\,\Delta\Psi} \int \frac{B^2}{B_p}\,dl$$

or since $I(\Delta\Psi) = j_{\parallel} A_{\perp} = j_{\parallel} q \Delta\Psi/B$,

$$\eta = \left(\frac{B}{j_{\parallel}}\right) \frac{V_{\parallel}}{\int \frac{B^2}{B_p} dl}$$

$$= \frac{B \cos a}{j_{pol}} \frac{V_{\parallel}}{\int \frac{B^2}{B_p} dl}$$

This equation is used to obtain η from measured data. Here a is the angle between B_p and B (Figure 4-3). The integral in the denominator is evaluated by a computer program from the vacuum flux plot (Figure 4-4). B is the total magnetic field at the point where the current density is measured.

F. RESISTIVITY DATA AND CONCLUSIONS

We made resistivity measurements in poloidal ohmic discharges as described in the previous section for a wide range of B_p, poloidal loop voltage, and initial

Figure 4-3. cos a and $\cos^2 a$ on the midplane as a function of distance from the major axis for various values of $\alpha = (B_T/B_p)_{MPOW}$. a is the angle between the poloidal magnetic field and the total magnetic field.

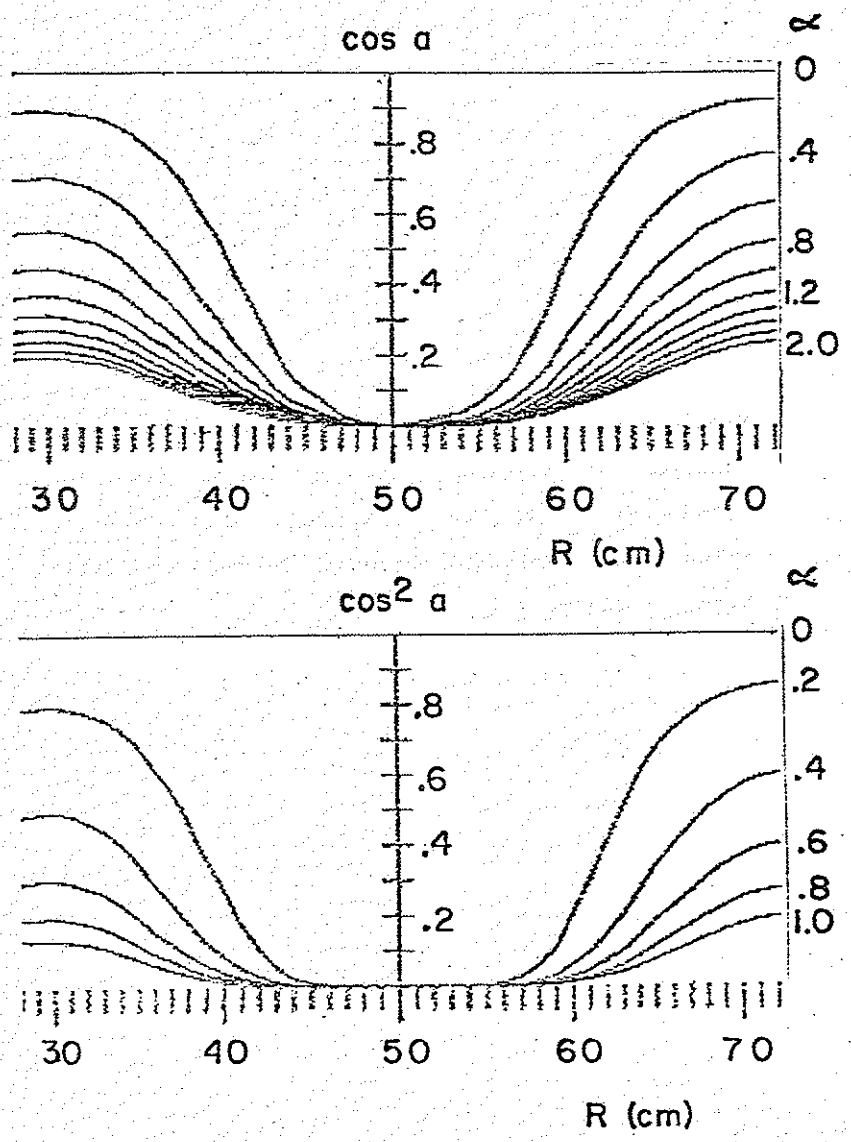

Figure 4-4. $\int \frac{B^2}{B_p} dl$ once around poloidally as a function of flux surface Ψ for various values of α, for a poloidal bank of 30 capacitors charged to 5 kV. The integral goes to infinity on the separatrix where B_p goes to zero.

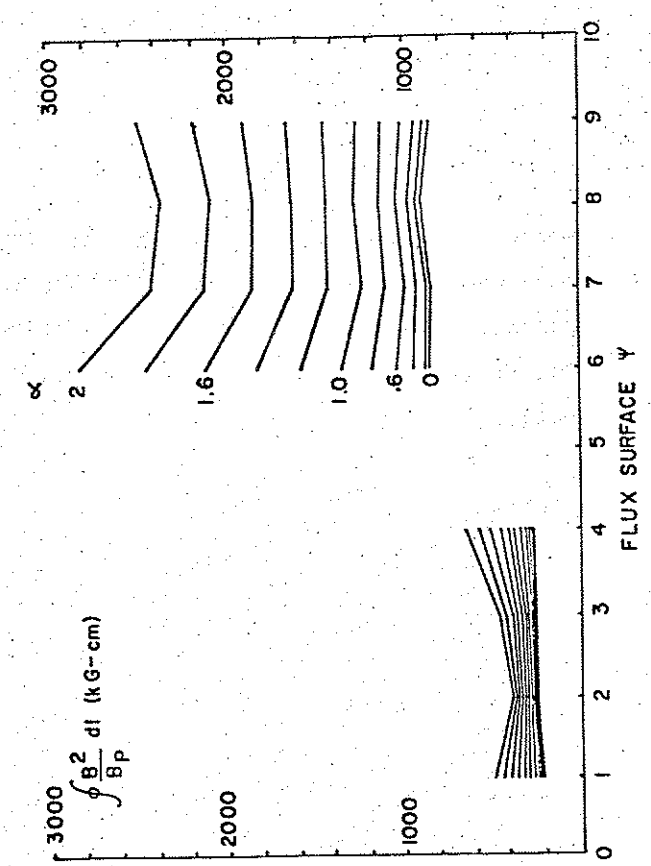

gas pressure values. Most of the measurements were made near the location of peak current and near the time of peak current in order to get the cleanest signals. The measured resistivity varied from approximately η_{Sp} to about 1500 x η_{Sp}.

The magnitude of the observed resistivity varies from ~ 10^{-4} Ω-m to ~ 10^{-2} Ω-m. The corresponding time for current penetration can be found from

$$\tau_{skin} = \frac{\pi \mu_o}{\eta} \delta^2$$

where μ_o is the permittivity of free space and δ is the distance penetrated in meters. If δ is 5 cm (the approximate distance from the wall to the current peak) then at $\eta = 10^{-4}$ Ω-m, τ_{skin} ~ 100 μsec; at $\eta = 10^{-2}$ Ω-m, τ_{skin} ~ 1 μsec. For times much longer than this, the plasma appears resistive. Since the plasma current takes 500 μsec to rise to its maximum (and somewhat longer at higher resistivities) the soak-in is apparently not an important factor in determining the

current profile. In the cases where the toroidal field is not crowbarred, so that the poloidal loop voltage reverses polarity and then is abruptly turned off, the current should die away in roughly a skin time. The resistivity during this reversed-polarity heating is always higher than during the first heating peak, so that τ_{skin} here is probably on the order of a few μsec; thus the observed current decay time of < 50 μsec in this mode is consistent with the measured resistivity.

Figure 4-5 shows the resistivity enhancement, η/η_{Sp}, plotted against the plasma collisionality. The solid lines represent the mirror theory described in section B. The data is in good agreement except in the collisionless regime, where η/η_{Sp} continues to rise, in agreement with the measurements made previously by Lencioni, Etzweiler, and Brouchous. Since the fluctuation level during poloidal ohmic heating is always high, it appears reasonable to attribute this anomalous resistivity to scattering from fluctuations as Etzweiler and Brouchous did. Thus the resistivity agrees well with the mirror-limited Spitzer theory as

Figure 4-5. Variation of resistivity enhancement with collisionality measured during poloidal ohmic heating. The solid lines represent mirror-limited Spitzer theory for the extremes of applied electric field.

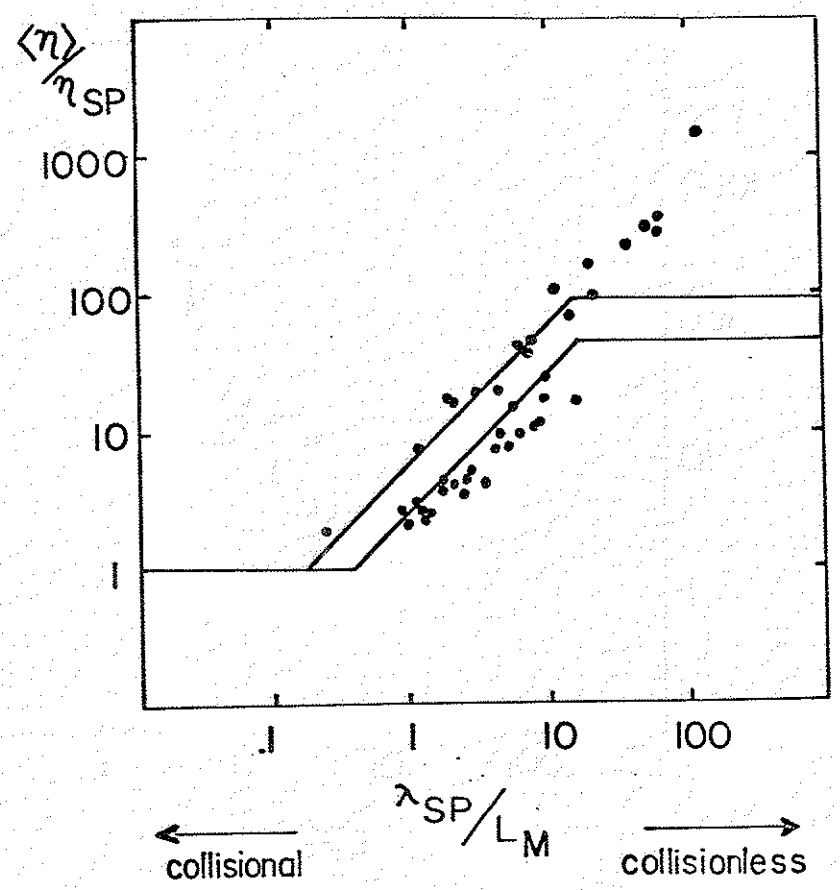

modified by previous experimenters to include fluctuations.

The applied electric fields $\langle E_{\parallel} \rangle$ range from about 10^{-2} x E_c to slightly above E_c. The appropriate electric field to consider here is the poloidal once-around average, since the plasma's collisionality is low enough that the streaming electron generally makes one or more poloidal transits before it is scattered. Figure 4-6 shows the variation of η/η_{Sp} with applied field E/E_c; the parameter range here is similar to that in Figure 4-5. The resistivity ratio appears to increase slightly faster than linearly with E/E_c.

Figure 4-7 shows the resistivity η as a function of electron density n_e at the location of peak current. The resistivity scales roughly as n_e^{-1}. The same scaling was observed by Lencioni and Etzweiler and contrasts with the $n_e^{-1/2}$ scaling predicted by Buneman for $E >> E_c$ (shown as solid line $\eta_{Buneman}$.) At low densities, corresponding to the largest values of E/E_c, the magnitude of the resistivity approaches the value predicted by Buneman.

Figure 4-6. Resistivity enhancement in poloidal ohmic heating as a function of applied electric field.

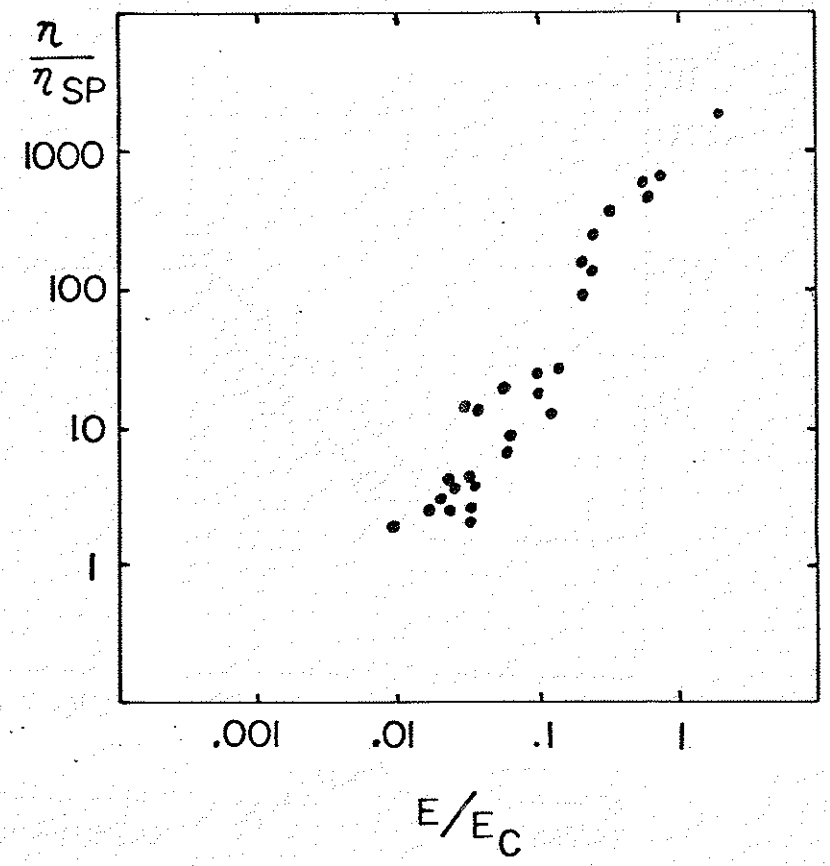

Figure 4-7. Magnitude of resistivity versus density at location of current peak during poloidal ohmic heating. The calculations for $\eta_{Demidov}$ assume a distance to the wall of r = 4.5 cm.

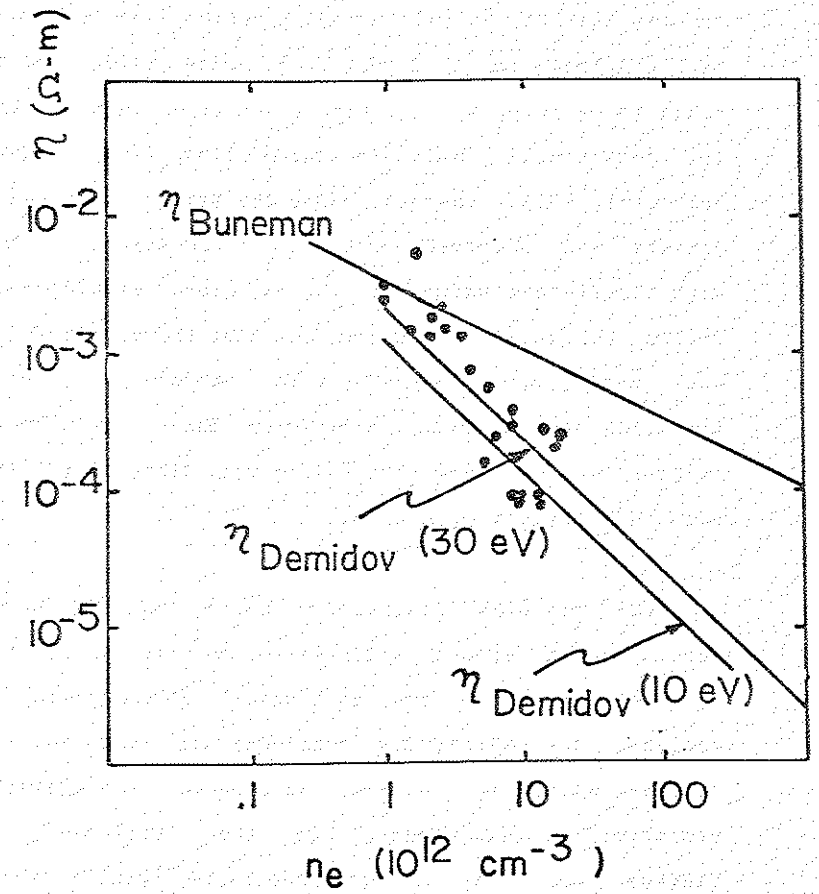

The other solid lines in Figure 4-7 represent Demidov's resistivity calculation with r = 4.5 cm and with T_e = 10 eV and T_e = 30 eV. (The distance from the current peak to the wall actually varies from ~6 cm in the midplane to ~ 2 cm in the bridge region, and T_e tends to be lower for the higher densities than for the low densities.) Demidov's calculation fits the data reasonably well. However, since the same scaling with density was observed by Lencioni[3] and Etzweiler[4] but with a different value of r, not much significance should be attached to the fact that the magnitude of the resistivity agrees with Demidov's theory. Etzweiler found that resistivity data from several machines did not show the scaling with distance to the wall that Demidov predicted.

The measured resistivity during poloidal ohmic heating thus agrees well with the mirror-limited Spitzer theory in the collisional and intermediate regimes. The resistivity continues to rise as the collisionality is lowered, as expected from previous resistivity measurements in the presence of fluctuations. The measurements during poloidal ohmic heating agree with previous resistivity measurements

made by Lencioni, Etzweiler, and Brouchous. As a plasma heating scheme, poloidal ohmic heating does appear to offer the hoped-for ability to couple large amounts of power into the plasma at modest values of current density.

REFERENCES FOR CHAPTER FOUR

1. L. Spitzer, Physics of Fully Ionized Gases (John Wiley and Sons, New York, 1962)

2. L. Spitzer and R. Härm, Phys. Rev. 89, 977 (1953)

3. D.E. Lencioni, Ph. D. Thesis, University of Wisconsin PLP 276 (1969)

4. J. Etzweiler, Ph. D. Thesis, University of Wisconsin PLP 738 (1977)

5. D. Brouchous and J. Etzweiler, Phys. Fluids 23(12), 2547 (1980)

6. J.F. Etzweiler and P.K. Smith, University of Wisconsin PLP 715 (1977)

7. P.K. Smith, University of Wisconsin PLP 682 (1976)

8. A. Gilardini, Low Energy Collisions in Gases (John Wiley and Sons, New York, 1972)

9. F.F. Chen, Introduction to Plasma Physics (Plenum Press, New York, 1974)

10. L.S. Frost, J. Appl. Phys. 32, 2029 (1961)

11. L.C. Johnson, Princeton Plasma Physics Laboratory, MATT-494 (1966)

12. H. Dreicer, Phys. Rev. 115, 238 (1959)

13. H. Dreicer, Phys. Rev. 117, 329 (1960)

14. O. Buneman, Phys. Rev. 115, 583 (1959)

15. B. Coppi and E. Mazzucato, Phys. Fluids 14, 134 (1971)

16. T.E. Stringer, Plasma Physics 6, 267 (1964)

17. D.F. Smith and J.V. Hollweg, J. Plasma Phys. 17, 105 (1977)

18. K.W. Gentle, G. Leifeste, and R. Richardson, Phys. Rev. Letters 40(5), 317 (1978)

19. R.Z. Sagdeev, Adv. in Plasma Physics vol. 5 (A. Simon and W.B. Thompson, eds., Wiley Interscience, N. Y., 1974), pp. 153-166.

20. D.E. Lencioni, Phys. Fluids 14, 566 (1971)

21. B.A. Demidov, N.I. Elagin, D.D. Ryutov and S.D. Fanchenko, Sov. Phys. JETP 21, 302 (1965)

22. W.C. Guss, Ph. D. Thesis, University of Wisconsin PLP 689 (1976)

23. S.M. Hamberger and M. Friedman, Phys. Rev. Lett. 21, 674 (1968)

24. B.A. Demidov, N.I. Elagin, and S.D. Fanchenko, Sov. Phys. Doklady 12, 467 (1967)

25. S.M. Hamberger and J. Jancarik, Phys. Fluids 15(5), 825 (1972)

26. K.W. Gentle, R. Bengston, J. Jancarik, T. Kocnanski, D. Patterson, P. Phillips, and R. Stinnett, Phys. Fluids 22(8), 1558 (1979)

27. D.A. Brouchous, to be submitted to Phys. Fluids

28. A somewhat different derivation was presented in reference 5.

CHAPTER FIVE: FLUCTUATIONS AND TRANSPORT

A. OCTUPOLE CONFINEMENT AND DIFFUSION

Confinement times ranging from tens of Bohm times to roughly the classical confinement time have been observed in octupole experiments. Since confinement times close to τ_{Bohm} will make an octupole Proof-of-Principle experiment impossible and will certainly make an octupole reactor unfeasible,[1] it is important to know how poloidal ohmic heating affects the confinement.

Particle confinement is usually discussed in terms of the diffusion coefficient D defined by Fick's Law

$$\vec{\Gamma} = n \langle \vec{v} \rangle = -D \vec{\nabla} n$$

where $\vec{\Gamma}$ is the flux of particles per unit area per unit time caused by the density gradient $\vec{\nabla} n$ and $\langle \vec{v} \rangle$ is

the mean particle velocity. In a strong uniform magnetic field, the particles gyrate around field lines until they experience collisions. After a collision, the particles begin gyrating around a new field line which is typically a gyroradius away from the original field line. This leads to a diffusion coefficient[2]

$$D_{class} = \rho^2/\tau = \frac{k T \nu_c}{m \omega_c^2}$$

where ρ is the gyroradius, τ is the mean time between collisions = $1/\nu_c$, and ω_c is the cyclotron frequency. The form $D \sim (\Delta x^2)/t$ is characteristic of a random-walk process such as classical diffusion. If the step size Δx is increased above ρ or if the time between collisions is decreased, D will be enhanced above D_{class}. Note that particles in a tokamak experience $\vec{\nabla} B \times \vec{B}$ forces which have a radial component and effectively enhance the step size Δx giving rise to so-called "neoclassical" diffusion; in an octupole with no toroidal field, these forces have no radial

component and so do not enhance the radial diffusion above classical.

Fluctuating electric fields in the plasma can cause particle drifts which enhance the transport. If the electric field E remains correlated for a typical distance L, particles acquire drift velocities $v_d \sim E/B$ which change direction after the particle has drifted a distance $\sim L$. This yields[3] $D_{turb} \sim EL/B$. If the fluctuation energy is of the same order as the particles' thermal energy, $eEL \sim kT$, then the diffusion coefficient becomes $D_{turb} = kT/eB$. This formula (with a numerical factor) was first given, without a derivation, by Bohm:[4]

$$D_{Bohm} = \frac{k\,T_e}{16\,e\,B}$$

Other collective phenomena such as convective cells,[5] which are closed contours of constant potential that cause a vortex $\vec{E} \times \vec{B}$ motion, can also enhance the

diffusion above classical and give rise to a different scaling with machine and plasma parameters.

Energy loss through diffusion can be treated similarly to particle diffusion. If there is no particle flux, the heat flux due to a temperature gradient is given by

$$q = K_e \frac{\partial T}{\partial x}$$

with $K_e \sim n\,D$ the heat conduction coefficient.[3]

Except for special cases, it is difficult to solve these diffusion equations for a multipole geometry with temperature and density gradients that vary arbitrarily in space and time. In order to compare observed density profiles and decay times with diffusion theory, the diffusion equation is usually set up in multipole coordinates with some simplifying approximations and solved as an eigenvalue problem.[6,7,8] The density profile shape, density decay time, and dependence on

machine parameters can then be used to infer the particle diffusion scaling law and magnitude. Most of the multipole diffusion work has involved particle transport rather than heat transport.

Good summaries of confinement data from multipoles, spherators, and levitrons appear in references 6 and 9. With a purely poloidal field and collisional plasmas, diffusion coefficients as small as a few times classical, and which scale as D_{class}, have been observed. When shear is added by adding a toroidal field and the plasma is not very collisional, the GA Octopole[15] and UW Levitated Octupole exhibit Bohm scaling but with coefficients usually $\sim 10^{-2}$ D_{Bohm} to $\sim 10^{-3}$ D_{Bohm}. Without shear, the Levitated Octupole usually sees diffusion several thousand times D_{class} which scales as predicted by Okuda and Dawson.[5] This is believed due to convective cells created upon plasma injection: the pulsed UW machine does not allow enough time for these cells to damp out, while the GA Octopole, which usually observed $\sim D_{class}$, was a D.C. machine. While the ultimate importance of the diffusion scaling with added toroidal field is not clear, Chen[6] concludes that "with poloidal field alone,

a gentle plasma production mechanism may allow D to be as small as D_c [classical] or D_{OD} [Okuda-Dawson] which would be small enough for reactor purposes."

B. EXPERIMENTAL CONFINEMENT DURING POLOIDAL OHMIC HEATING

During poloidal ohmic heating it is difficult to measure in a direct way the particle confinement but fairly simple to measure the energy loss rate; after the heating stops, the particle confinement time can be measured by observing the plasma decay, while the energy confinement is difficult to measure. Thus it is difficult to accurately determine the effect of poloidal ohmic heating on confinement. In practice, however, even a rough comparison indicates that poloidal ohmic heating significantly reduces the confinement time.

The ohmic input power to the plasma is calculated by integrating the product of the measured poloidal current density and the calculated poloidal electric field over the machine volume. This input power ranges

up to ~2 MW in these experiments. The plasma energy is given by $E = 3/2\ Nk(T_e + T_i) \sim 3/2\ NkT_e$, where N is the total number of electrons. (The ions are assumed cold; except at the highest densities in these experiments, the electron-ion equilibration time[17] is longer than the duration of the experiment.) Figure 5-1 shows the typical variation of electron temperature, total poloidal plasma current, and electron density with poloidal loop voltage V_{TG}. Note that the electron temperature saturates at $T_e \lesssim 30$ eV while the plasma density and plasma current continue to rise. Figure 5-2 shows total plasma energy as a function of peak ohmic input power. There is little increase in plasma energy above $P_{in} \sim 1$ MW; this is a reflection of the temperature and density saturation. Even well below this saturation, the energy confinement time τ_E (plasma energy divided by ohmic input power) is quite low, ~ 30 μsec. At the highest ohmic powers used, τ_E drops to about half this value. Note also that τ_E appears to be independent of the poloidal magnetic field from these data; however, since the plasma parameters change as the poloidal field is varied, it is not simple to infer a scaling law for the diffusion coefficient from this.

Figure 5-1. Electron temperature (T); electron density (n); and poloidal plasma current (i) as functions of poloidal loop voltage V_{TG}. The electron temperature is measured with a triple probe and confirmed by measuring oxygen line radiation ratios; the density is measured with a volume-averaging Langmuir probe checked against the 70 GHz interferometer. The poloidal bank voltage was held constant at 2.0 kV for these data.

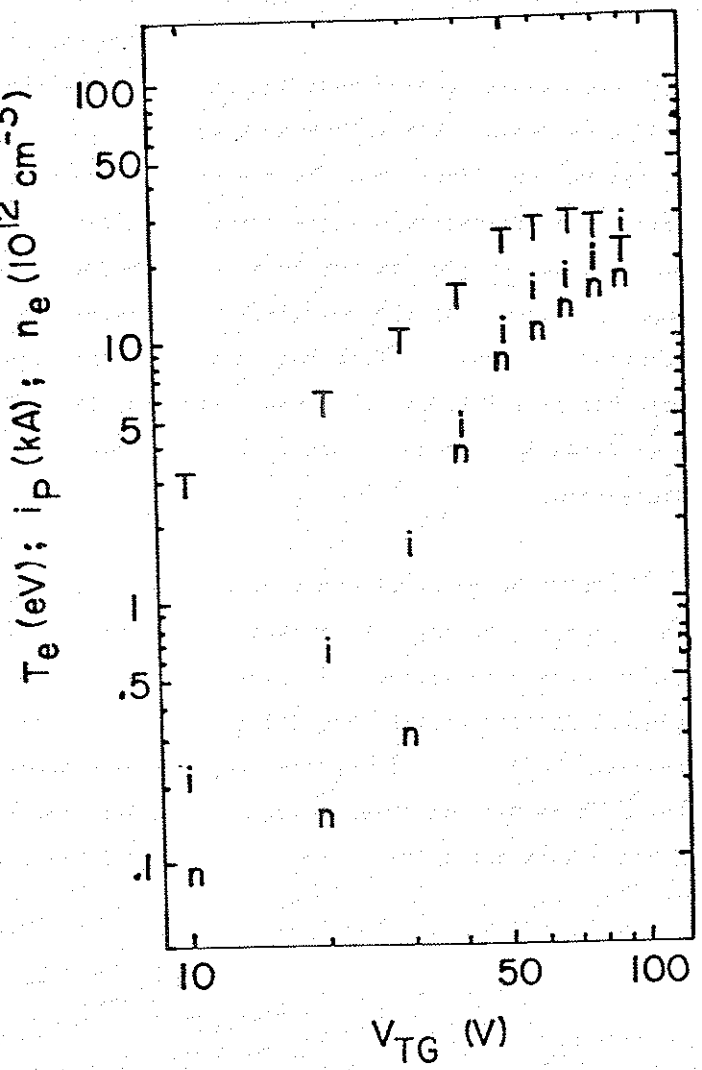

Figure 5-2. Plasma energy (3/2 $N_e kT_e$) as a function of ohmic input power for two values of poloidal magnetic field. (These data are not from the same data run as Figure 5-1)

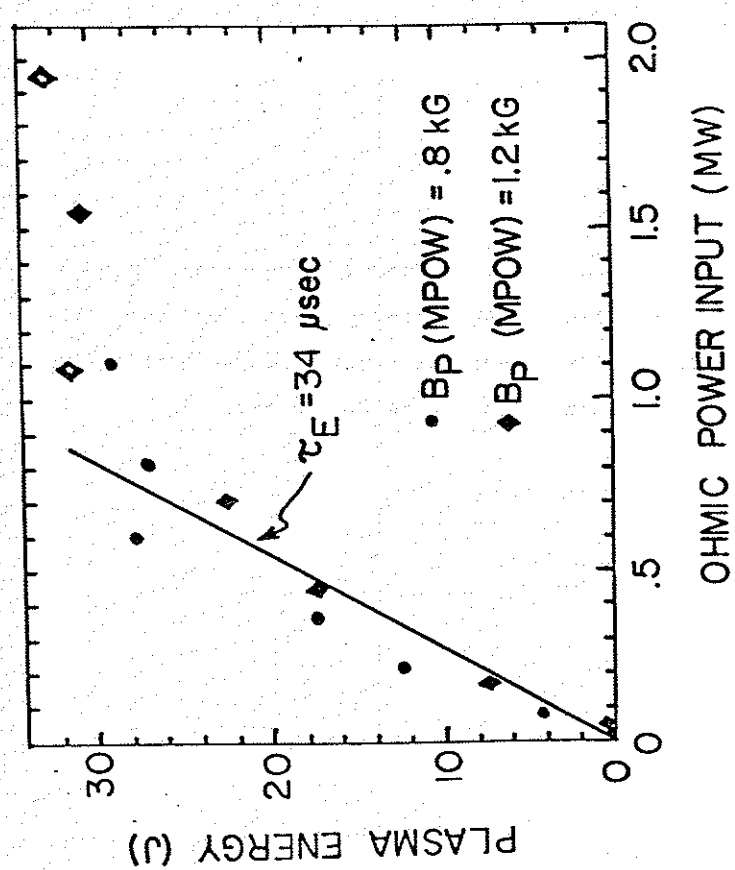

Measurements of impurity radiation, as mentioned in chapter 3, show far too little radiation to account for the short energy confinement time. The impurity radiation signals are always much weaker (typically by a factor of five) than in the standard tokamak-type Tokapole II discharges, where impurity radiation is not the dominant energy loss process, even though the ohmic input is higher for the poloidal ohmic discharges. The measured energy confinement time for Tokapole II operated as a tokamak is about 100 to 300 μsec,[10] significantly longer than for the poloidal ohmic discharges.

After the poloidal ohmic heating is turned off, the plasma density is peaked on the separatrix and decays with a characteristic time of about 2 msec. A typical density profile evolution late in time is shown in Figure 5-3. This is easily compared with theory for the case of Bohm diffusion: assuming a flat temperature profile constant in time and assuming a density profile

$$n(\Psi) = n_o \cos\left(\frac{\pi(\Psi - 5)}{2(\Psi_{crit} - 5)}\right)$$

Figure 5-3. Density profiles on the midplane late in time. The toroidal field is crowbarred; the poloidal current has decayed almost to zero at 3 msec. The poloidal bank voltage is 2.0 kV, toroidal bank voltage 3.0 kV. The solid line shown at t = 4 msec represents the function

$$n = n_o \cos\left(\frac{\pi\,(\Psi - 5)}{2(\Psi_{crit} - 5)}\right)$$

normalized to the measured peak density.

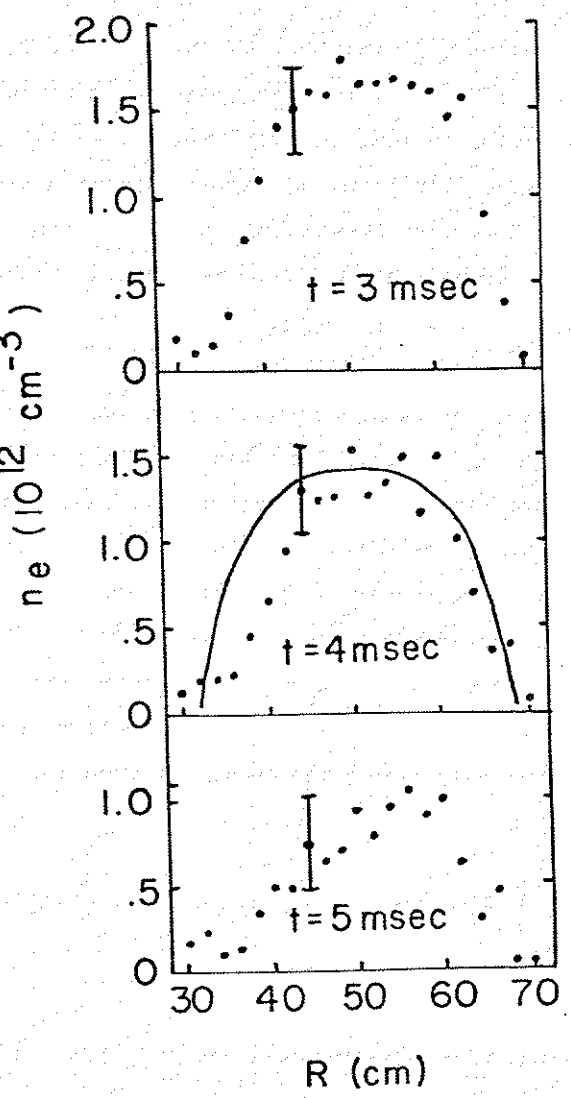

which reasonably approximates the measured density profile (Figure 5-3), the density profile decays exponentially in time without significantly changing shape. The calculation of Meade[11] yields a decay time of ~ 200 μsec for this case, so that the observed density decay after the heating is turned off corresponds to $D \sim 0.1\ D_{Bohm}$.

During the heating the diffusion constant cannot be found in this way since the density profile is not even approximately an eigenmode of the diffusion equation, as the cosine function above is; also, there is now a power source in the equation. We used H. Garner's computer program TEVOL[13,14] to get an approximate diffusion coefficient from the measured τ_E. TEVOL is a temperature evolution code which solves the electron energy transport equation

$$\frac{3}{2}\frac{\partial}{\partial t}(n_e T_e) + \vec{\nabla}\cdot(K_e \vec{\nabla} T_e) = Q(\Psi)$$

in an octupole, assuming toroidal symmetry. The ohmic

power input $Q(\Psi)$, density profile $n_e(\Psi)$, and initial temperature profile $T_e(\Psi, t=0)$ are specified, along with the diffusion constant and its scaling law. The program produces temperature profiles $T_e(\Psi, t)$ as its output.

To simulate the ohmic heating case, TEVOL was run with an experimentally measured density profile and with 1 MW of ohmic input power at a location corresponding to the poloidal current peak. The diffusion was assumed to obey Bohm scaling. The magnitude of the diffusion constant was adjusted until it produced a temperature profile ~ constant in time at $T_e \sim 25$ eV, corresponding to the measured temperature (Figure 5-4). The best choice for the diffusion coefficient was found to be $D \sim 1.5 - 2.5\ D_{Bohm}$. For $D \sim 2\ D_{Bohm}$, the program calculated an energy confinement time $\tau_E = 42$ μsec, in agreement with the observed $\tau_E \sim 30$ μsec. Thus for Bohm diffusion scaling, the measured T_e, τ_E, and n_e profile indicate $D \sim 2\ D_{Bohm}$ during the poloidal ohmic heating.

Figure 5-4. a) Experimental density profile $n_e(\Psi)$ used in TEVOL code. Also shown (P_{OH}) is location of 1 MW input power specified in code. The input power is constant in time. The code is written for the Wisconsin Levitated Octupole, so that the flux coordinates do not correspond exactly to those of Tokapole II; $\Psi_{crit} \sim 7.5$ compared to $\Psi_{crit} \sim 8.2$ in Tokapole II. The density profile has been adjusted to compensate for this.

b) Initial temperature profile specified in TEVOL code.

c) Temperature evolution T_e (Ψ,t) calculated by TEVOL using $D = D_{Bohm}$. The temperature rises in time, indicating the diffusion constant chosen is too small.

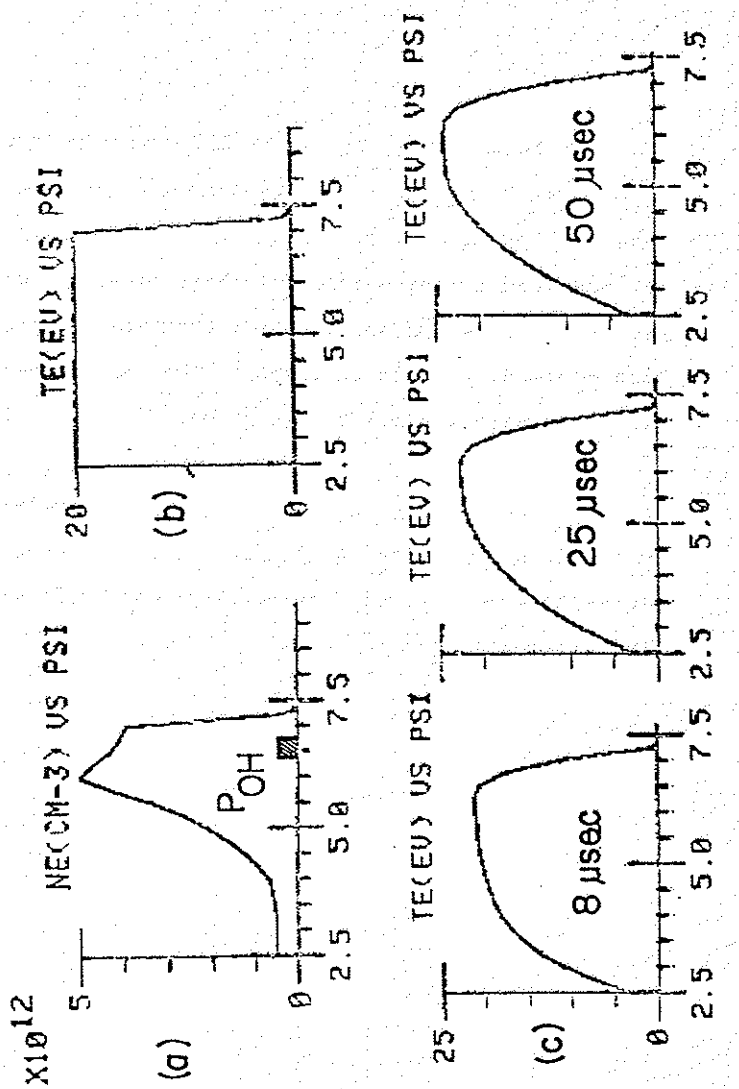

d) Temperature T_e (Ψ,t) calculated by TEVOL using D = 2 D_{Bohm}. The temperature remains constant in time. Also shown are temperatures T_e (Ψ) measured during a poloidal ohmic heating case with P_{in} ~ 1 MW, adjusted to the Levitated Octupole flux coordinates used in TEVOL. The measurements were made with a small triple probe.

e) Temperature evolution T_e (Ψ,t) calculated by TEVOL using D = 4 D_{Bohm}. The temperature decreases in time, indicating the diffusion constant chosen is too large.

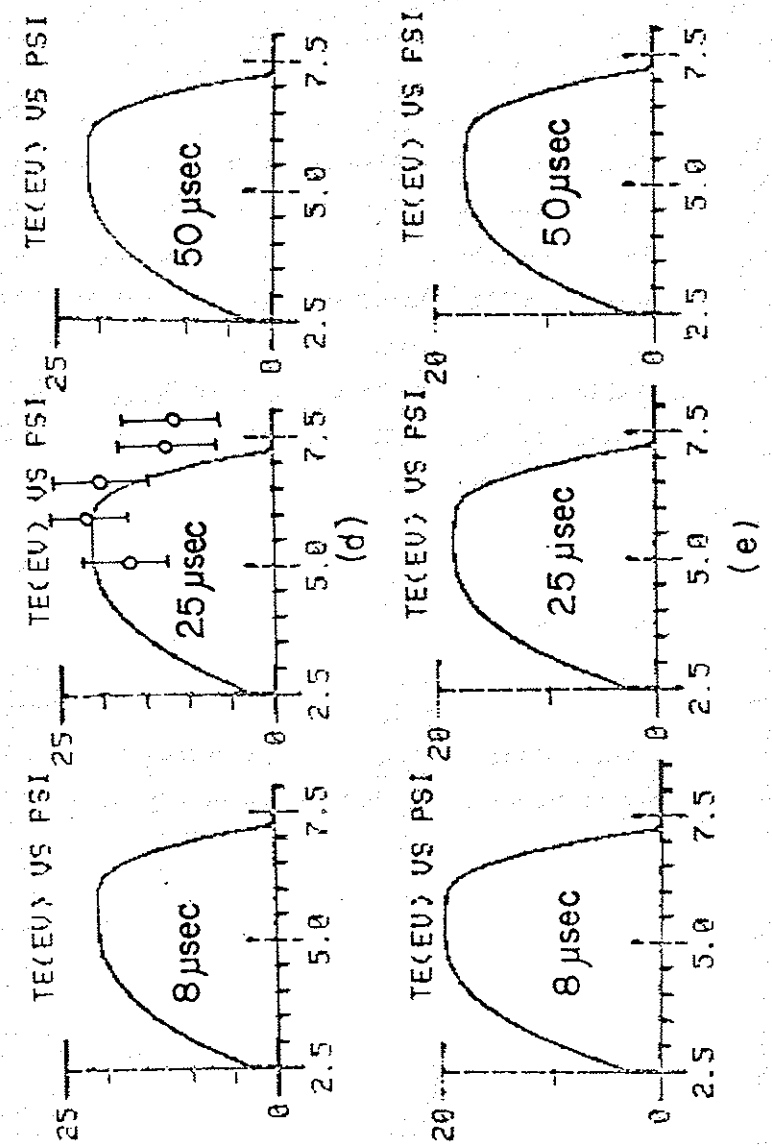

While $D \sim 2\, D_{Bohm}$ is a typical value obtained from measurements during poloidal ohmic heating, the diffusion coefficient does not appear to scale as D_{Bohm}. τ_E measurements covering a broad range of plasmas produced by poloidal ohmic heating indicate diffusion coefficients ranging from $D \sim D_{Bohm}/2$ to $D \sim 6\, D_{Bohm}$ and do not show a simple dependence on plasma or field parameters such as that predicted by D_{Bohm} or D_{class}.

C. EFFECT OF FLUCTUATIONS ON TRANSPORT

Electric fields in a plasma give rise to particle drifts with velocity $v = E_\perp / B$, where $E_\perp$ is the electric field perpendicular to B. This gives a particle flux

$$\Gamma = \frac{\langle n\, E_\perp \rangle}{B}$$

If n and $E_\perp$ are separated into DC parts n_o, $E_{\perp o}$ and oscillating parts δn, $\delta E_\perp$, then the flux is

$$\Gamma = \frac{\langle n_o\, E_{\perp o} \rangle}{B} + \frac{\langle \delta n\, \delta E_\perp \rangle}{B}$$

where the cross terms have averaged out to zero. In the poloidal ohmic heating experiments the first term is negligible compared to the second term and so we ignore it. The second term gives an average particle velocity

$$\langle v \rangle = \frac{\langle \delta n\, \delta E_\perp \rangle}{n B}$$

due to the fluctuating electric fields. The diffusion constant D is thus

$$D = \frac{\langle \delta n\, \delta E_\perp \rangle}{B \nabla n}$$

Thus if the phase and amplitude of the density and electric field fluctuations are known one can calculate a particle diffusion rate. This method is often used to measure diffusion rates in the UW octupoles.[8,12]

During poloidal ohmic heating, fluctuation levels are very high in the region of current flow. The density fluctuation level $\delta n/n$ is approximately 100% in this region (see Figure 2-6) as long as significant plasma current is present, even at very low poloidal loop voltages (Figure 5-5).

In order to correlate density fluctuations with electric field fluctuations, a small 3-tipped probe was used to make both measurements simultaneously. Two of the tips were aligned perpendicular to B and monitored with a differential amplifier to give the local electric field $\delta E_\perp$; the third tip was biased to give the local ion saturation current. Figure 5-6a shows typical sets of waveforms obtained in this way. (Because of field line tilt, only the first ~1 msec of the electric field signal is significant). Note that the $\delta E_\perp$ signal and the δj_{sat} signal are 180° out of phase. The orientation of the fields was such that

Figure 5-5. Ion saturation current (j_{sat}) signal and fluctuation level ($\delta j_{sat}/j_{sat}$) as functions of poloidal loop voltage V_{TG}. The poloidal field was held constant at a bank voltage of 2.0 kV. The data were taken with a Langmuir probe at R=67 cm on the midplane. Typical error bars are shown.

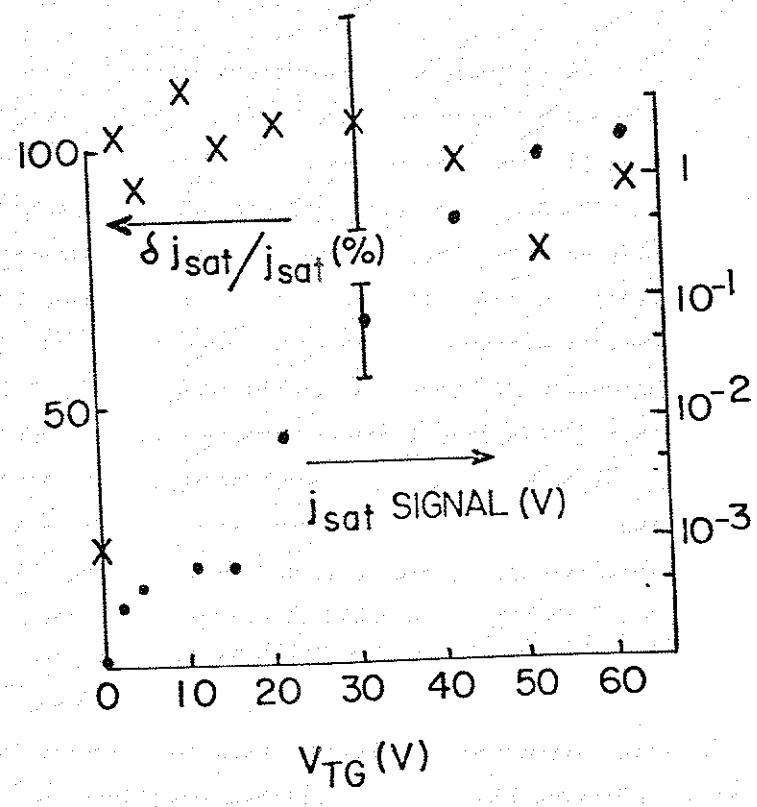

Figure 5-6. a) Local electric field perpendicular to B and local j_{sat} fluctuations measured with a small (.25 cm between tips) three-tipped Langmuir probe located at R = 67 cm on the midplane. The j_{sat} signal has been passed through a 1 kHz, 6 dB/octave high-pass filter; the peak-to-peak fluctuation amplitude on this signal is ~ 100% of the averaged j_{sat}. The scale on the electric field traces is 8 V/cm per box. The electric field signal has not been filtered, since its DC value is negligible. The horizontal scale is .2 msec/box. Only the first ~1 msec of the $\delta E_\perp$ trace is significant since after this the field lines are pitched so much that the measured E is no longer perpendicular to B.

b) Perpendicular electric field fluctuation level (averaged over the duration of the ohmic heating pulse) as a function of poloidal bank voltage V_p and as a function of poloidal loop voltage V_{TG}.

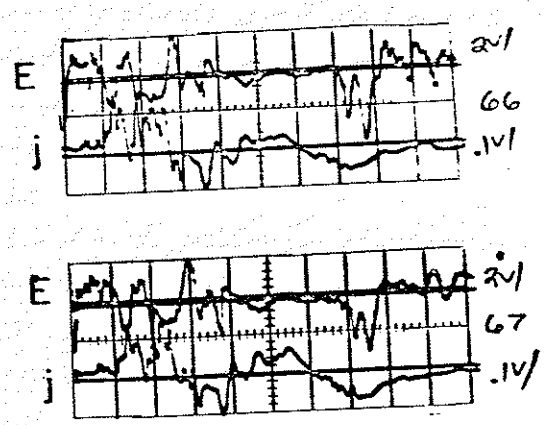

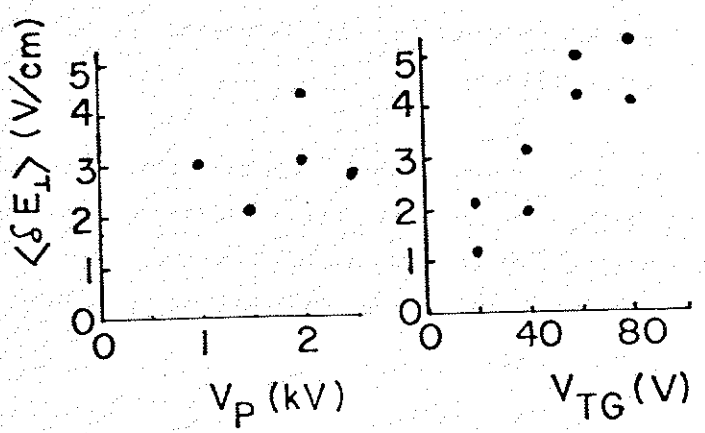

these measurements indicate an outward particle flux $\vec{\Gamma}$.

An estimate of the particle diffusion can be made from data such as those in Figure 5-6a. Assuming the j_{sat} fluctuations represent $\delta n/n$ of 100% and that δn and $\delta E_\perp$ are 180° out of phase, averaging the fluctuations over the duration of the current pulse yields a $\langle v \rangle$ of $\sim .3 \times 10^6$ cm/sec. Taking 5 cm as a typical distance to the wall then gives as a crude estimate of particle confinement time $\tau_p \sim 17$ μsec. This is the same order of magnitude as the observed $\tau_E \sim 30$ μsec. Combining the observed density gradient at the time of peak current with the $\langle \delta n \, \delta E_\perp \rangle$ measurements yields a diffusion coefficient of $D \sim 1.5 \times 10^6$ cm^2/sec. As shown in Figure 5-5b, the electric field fluctuations $\langle \delta E_\perp \rangle$ increase with applied electric field and have no obvious dependence on B_p. The values calculated from these measurements are very approximate due to shot-to-shot variations and due to averaging the quantities over the duration of the ohmic heating; also, because this is a local measurement, it is difficult to compare with the diffusion coefficients

calculated by observing the overall density profile decay after the heating is turned off.

The diffusion coefficient from Bohm's formula at the temperature (~25 eV) and poloidal field (~1 kG) corresponding to Figure 5-6a is $D_{Bohm} \sim 2 \times 10^5$ cm^2/sec, while the classical value is ~ $D_{class} = 60$ cm^2/sec. The fluctuation data indicate a local diffusion coefficient more than 10^4 times classical and about eight times greater than D_{Bohm}. This measurement of the local diffusion coefficient in the region of large fluctuations appears reasonably consistent with the overall coefficient $D \sim 2 D_{Bohm}$ calculated by TEVOL. Finally, note that if $\delta n/n$ is constant and maintains its phase relation with $\delta E_\perp$, then Bohm's diffusion formula predicts that $\langle \delta E_\perp \rangle$ will remain constant as B_p is varied; this is consistent with Figure 5-5b, although the data are not conclusive.

The fluctuations produced by poloidal ohmic heating thus appear to increase the particle diffusion to a value several times D_{Bohm}, giving a particle confinement time which is on the order of the observed energy confinement time. The large electric field

fluctuations indicate that the poloidal ohmic heating used in these experiments is not a "gentle plasma production mechanism."

D. EFFECT OF LOCALIZED POWER DEPOSITION

Even if poloidal ohmic heating did not cause fluctuations that enhance the diffusion, it would yield a shorter energy and particle confinement time than that of an octupole with density and temperature peaked on the separatrix. This is because poloidal ohmic heating couples most of the power to the outside edge of the plasma, where it can quickly diffuse to the wall.

If the diffusion process obeys classical scaling, diffusion times should scale as the magnetic flux to be diffused across. This follows directly from the random-walk nature of classical diffusion, which gives an average distance travelled proportional to the number of steps taken; and from the classical assumption of step size $\Delta x \propto 1/B$.

The poloidal ohmic heating input power in Tokapole II peaks at $\tilde{}\ \Psi = 7$; if we assume the plasma is lost when it reaches the critical flux surface $\Psi_c = 8.2$, then confinement times should be about 7 times shorter during poloidal ohmic heating than for similar octupole plasmas peaked on the separatrix ($\Psi = 5$). This estimate is confirmed by comparing results of the TEVOL code for plasmas with the temperature and density peaked on the separatrix with cases where n_e and T_e are peaked at $\tilde{}\ \Psi = 7$; the location of the poloidal ohmic heating power gives confinement that is a factor of 5 to 10 worse than for standard octupole profiles peaked on the separatrix.

If the diffusion process obeys Bohm scaling, the effect of peaking the power at $\Psi = 7$ should be less pronounced, since D_{Bohm} has a weaker B-dependence than D_{class}. This is verified by a TEVOL calculation similar to that in section C, but with 1 MW of ohmic power put in at the separatrix and with a density profile peaked on the separatrix. To maintain a temperature profile constant in time for this case, it was necessary to increase D to $\tilde{}\ 8\ D_{Bohm}$, a factor of

four increase over the diffusion constant calculated with the ohmic power peaked at $\tilde{}\ \Psi = 7$.

Thus it appears that the poor confinement during poloidal ohmic heating is partially due to the unfavorable location of the ohmic input power, which degrades the confinement by a factor of four to ten. Enhanced transport due to fluctuations in the region of poloidal current flow reduces the confinement time by an additional factor of $\tilde{}$ two to five.

REFERENCES FOR CHAPTER FIVE

1. University of California at Los Angeles, University of Wisconsin, TRW Defense and Space Systems Group, A Proof-of-Principle of the Advanced Fuels Multipole-Surmac Concept, prepared for the Department of Energy, Office of Magnetic Fusion Energy (October 1978)

2. F.F. Chen, Introduction to Plasma Physics, Plenum Press, New York (1974)

3. S.I. Braginskii, Reviews of Plasma Physics, ed. M.A. Leontovich, Consultants Bureau, New York (1965)

4. D. Bohm, The Characteristics of Electrical Discharges in Magnetic Fields, ed. A. Guthrie and R.K. Wakerling, McGraw Hill, New York (1949)

5. E. Okuda and J.M. Dawson, Phys. Fluids 16, 408 (1973)

6. F.F. Chen, University of California at Los Angeles PPG-553 (1981)

7. G.A. Navratil, University of Wisconsin PLP 693 (1976)

8. D.M. Meade, Phys. Rev. Letters 17, 13 (1966)

9. G.A. Navratil and R.S. Post, Comments on Plasma Physics and Controlled Fusion 5, 2:29 (1979)

10. R.J. Groebner, Ph.D. Thesis, University of Wisconsin (1979)

11. D.M. Meade, University of Wisconsin PLP 71 (1966)

12. J. Schmidt, Ph.D. Thesis, University of Wisconsin PLP 250 (1969)

13. H.R. Garner, Bull. Am. Phys. Soc. 25, 967 (1980)

14. H.R. Garner, University of Wisconsin PLP 844 (1980)

15. T. Ohkawa, M. Yoshikawa, R.E. Kribel, A.A. Schupp, and T.H. Jensen, Phys. Rev. Lett. 24, 95 (1970)

16. T. Tamano, R. Prater, and T. Ohkawa, Phys. Rev. Lett. 30, 431 (1973)

17. L. Spitzer, Jr., Physics of Fully Ionized Gases (Wiley, New York, 1962) chapter 5

CHAPTER SIX : EQUILIBRIUM AND STABILITY

A. EQUILIBRIUM

A possible reason for the fluctuations which reduce the confinement during poloidal ohmic heating is that the heating upsets the octupole equilibrium. This seems unlikely because the fluctuations persist at levels of ~ 100% even when the plasma current and electron density are reduced to very low levels (Figure 5-5); at these low levels the perturbations produced by the plasma current and plasma pressure must be very small, while the poloidal field is not changed.

One could in principle detect the loss of plasma equilibrium experimentally by measuring the angle between the plasma current and the magnetic field. Since plasma equilibrium requires that the plasma pressure be balanced by the magnetic field force, $\vec{\nabla} p = \vec{J} \times \vec{B}$, an angle greater or less than the angle required for pressure balance implies a net force on the plasma, i.e. a loss of equilibrium. However, for

the pressure gradients in Tokapole II during poloidal ohmic heating, the maximum angle between $\vec{J}$ and $\vec{B}$ required for equilibrium is only ~ 3^{o}. Using a small movable Rogowski coil, this angle was found to be between $\pm$ 15^{o}, but because of the poor accuracy of these measurements they are inadequate to detect the absence of equilibrium.

In order to verify that the octupole equilibrium is not destroyed by the current densities and plasma pressures produced by poloidal ohmic heating, we used the equilibrium code TOPEC[1] written by M. Phillips. The code solves the Grad-Shafranov equation[2,3]

$$\Delta^{*}\Psi = -\mu_{o} R^{2} \frac{dp}{d\Psi} - I \frac{dI}{d\Psi}$$

where $2\pi\Psi$ is the poloidal flux function Ψ_{pol}; R is the distance to the major axis; $(2\pi/\mu_{o})I(\Psi)$ is the poloidal current between Ψ and the major axis; and $\Delta^{*} = R\frac{\partial}{\partial R}\frac{1}{R}\frac{\partial}{\partial R} + \frac{\partial^{2}}{\partial y^{2}}$, where y is the "vertical" direction, i.e. parallel to the major axis. The equation

expresses the pressure balance equation in terms of Ψ, assuming axisymmetry, with the three terms corresponding to $J_{T}B_{p}$, ∇p, and $J_{p}B_{T}$ respectively.

The measured poloidal current density as a function of distance from the major axis and the vacuum toroidal and poloidal field strengths are specified as inputs to the code. Figure 6-1 a shows a typical experimental current density profile. Starting with the vacuum flux surfaces, the program iterates to find the flux surfaces for which the Grad-Shafranov equation is satisfied with the experimental current density; the existence of such a solution confirms that the measured current density profile is consistent with MHD equilibrium. Figure 6-1 b shows the vacuum flux plot for the ring position assumed in the code. With the experimental current profile, the program quickly converges to an equilibrium flux plot (Figure 6-1 c) which is very similar to the vacuum flux plot. Thus the code demonstrates that the profiles produced by poloidal ohmic heating are consistent with an equilibrium in which the flux surfaces are changed very little by the plasma; the fluctuations seen experimentally are not due to loss of equilibrium.

Figure 6-1. a) Typical poloidal current density profile specified as input to TOPEC code. (Compare to Figure 2-8)

b) Vacuum poloidal flux plot from TOPEC code. The ring positions are slightly different from those in Figure 2-3.

c) Equilibrium flux plot generated by TOPEC code for current density profile in a. The flux surfaces shown correspond to those in b.

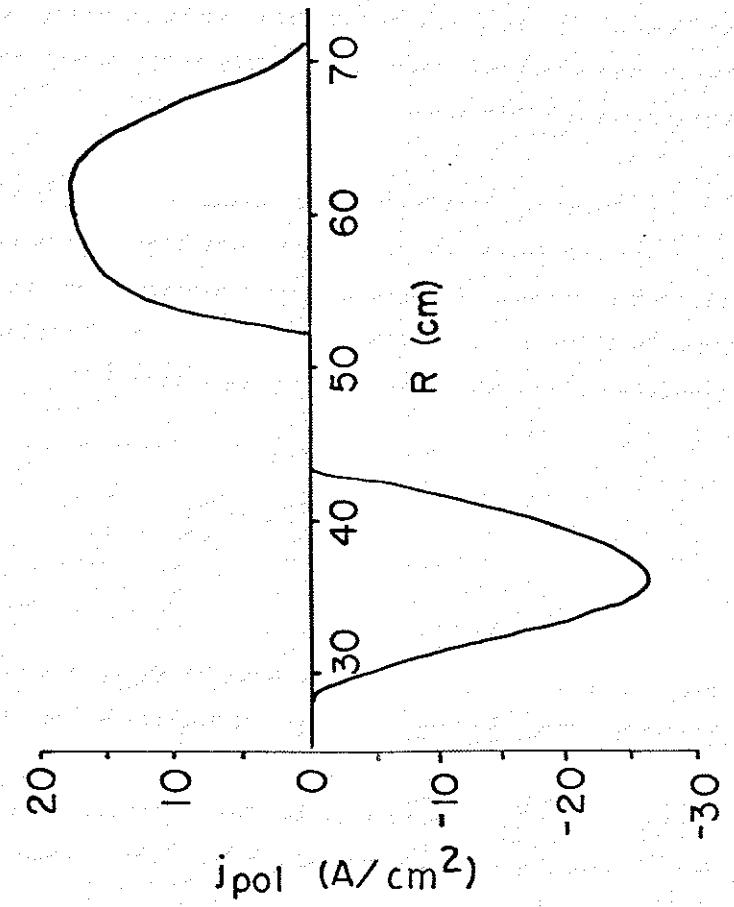

(b)

(c)

B. FLUCTUATION CHARACTERISTICS

As shown in Figure 6-2 (see also Figure 2-6), the density profile is initially peaked well outside the separatrix and gradually moves in to peak on the center. The condition for ideal MHD stability against interchange modes in a multipole is[4]

$$\vec{\nabla} p \cdot \vec{\nabla} \int \frac{dl}{B} > 0$$

where p is the plasma pressure and the integral is taken on a flux surface. This implies that for interchange stability inside Ψ_c, the pressure profile must be peaked on the separatrix, and thus one might expect a pressure-driven instability in the early stages of the poloidal ohmic discharge, when the density profile (and presumably the pressure profile) is inverted.

In fact, however, the fluctuation level does not depend on the direction of the density gradient (Figure 6-2); ion saturation current fluctuations are always on

Figure 6-2. Ion saturation current profile (solid circles) and fluctuation level $\delta j_{sat}/j_{sat}$ (boxes) at two different times during a poloidal ohmic heating shot. The toroidal bank voltage is 3 kV, poloidal bank voltage 2 kV.

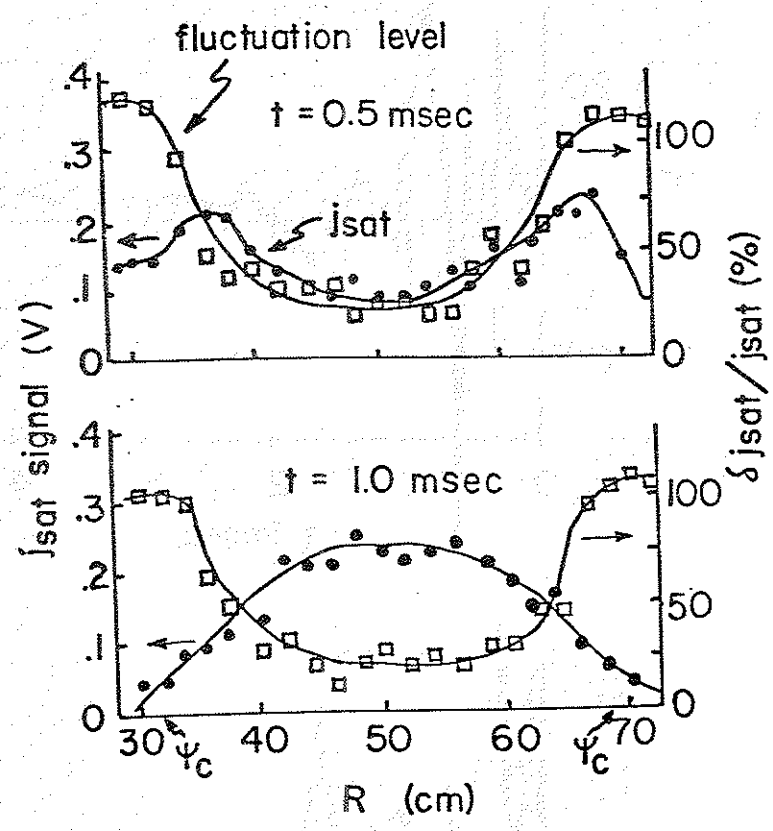

the order of 100% in the region where the plasma current flows. Thus it appears that the main source of energy for driving the fluctuations is the plasma current, rather than the plasma pressure.

Figure 6-3 a shows a typical trace of floating potential versus time near the region of peak current density. Figure 6-3 b shows the power spectrum of such a signal, computed by a Fast Fourier Transform program.[5] Note that there is no strongly dominant frequency peak, although a broad peak between f= 5 kHz and f= 10 kHz is usually seen. When averaged over many shots, the overall power spectrum has roughly a f^{-a} form, where $.7 < a < 1.5$. There is very little fluctuation energy above about 10 kHz.

We made some rough wavelength measurements in several cases where the 5 to 10 kHz peak was strong. The measurement is difficult because the field line pitch changes significantly during a fluctuation period. We used two Langmuir probes to look at the floating potential on the same flux surface, one on the midplane and one 15 cm above the midplane. The lower probe could be swivelled approximately $\pm 30^{o}$ about a

Figure 6-3. a) Typical floating potential signal as a function of time at r=67 cm in the midplane.

b) Typical power spectrum of floating potential signal.

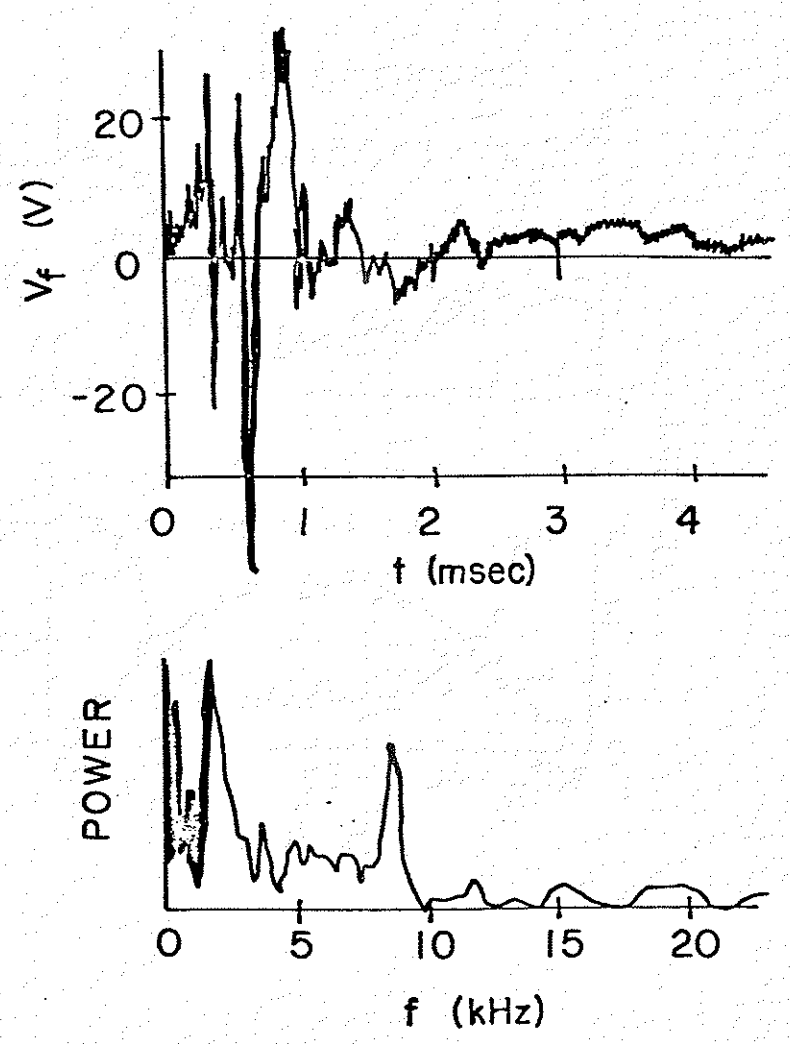

vertical axis so that its tip moved in a toroidal direction. The phase shift between the two signals as a function of time and of tip location was combined with the known field line pitch as a function of time to yield wavelengths parallel to and perpendicular to the magnetic field. The approximations used in making this calculation and the difficulty of making phase measurements on a noisy signal lead to large uncertainties in the measured wavelengths, probably on the order of ± 50%.

Calculations for the case shown in Figure 6-4 and for a few similar cases yield a $\lambda_\perp \sim$ 20 cm, $\lambda_\parallel \gtrsim$ 120 cm, with larger uncertainties in the parallel wavelength due to the small phase shift along a field line. Since the mode at 5 to 10 kHz is sometimes only weakly present in the fluctuations, it is not certain that these measurements are representative of the fluctuations in general.

The wave structure can also be specified in terms of the poloidal and toroidal components. With two floating potential probes spaced ~ 40 cm apart toroidally, we measured toroidal wavelengths λ_{tor}

Figure 6-4. Phase shift between the floating potential signals to two probes as a function of time for three positions of the upper probe tip. In A the upper tip is swivelled left ~ 30°; in B the upper tip is radial; and in C the upper tip is swivelled right ~ 30°. The lower tip is at r = 66 cm in the midplane, the upper tip on the corresponding flux surface ~ 15 cm above the midplane. The known field line pitch as a function of time allows calculation of $\lambda_\parallel$ and $\lambda_\perp$ from these phase shifts.

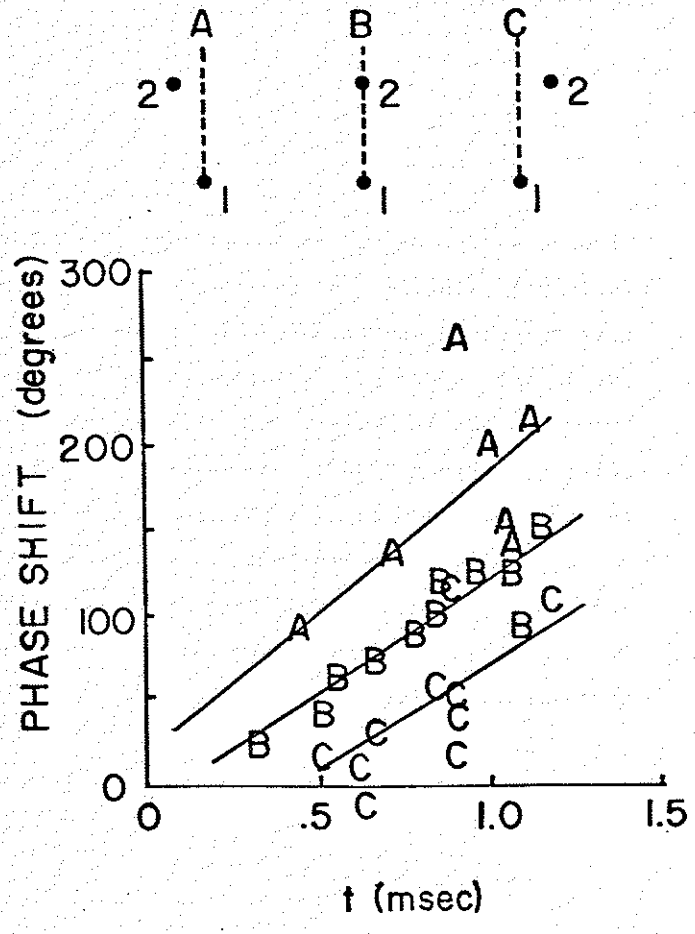

~ 60-80 cm; when the probes were spaced ~ 110 cm apart toroidally (90° toroidal angle), we could see little correlation between the two signals. Poloidal wavelength measurements generally showed poorer correlation but were consistent with wavelengths up to a few times the toroidal wavelength.

Figure 6-5 shows the ratios of these wavelengths plotted as $m/n = \frac{L_{pol}\ \lambda_{tor}}{L_{tor}\ \lambda_{pol}}$ as a function of time for three toroidal bank voltages, along with the calculated q's for the corresponding bank voltages. Here L_{pol} and L_{tor} refer to the distance around the machine poloidally and toroidally, respectively, on the given flux surface. The accuracy of these measurements was poor, since each point represents the period of only one cycle of the oscillation and since the signal correlation was not very good; but the data appear reasonably consistent with $q = m/n$. This is further indication that the fluctuations have a long parallel wavelength, since $\vec{k} \cdot \vec{B} = 0$ implies that $\frac{m}{r} B_p - \frac{n}{R} B_T = 0$, i.e. $q = m/n$.

Figure 6-5. Calculated safety factor q and measured mode number ratio m/n for three different toroidal bank settings as a function of time. In A the toroidal bank voltage is 2 kV; in B 3 kV; and in C 4 kV. The poloidal bank voltage is 2 kV in each case. The lower case letters represent measurements of the ratio of m/n (poloidal mode number / toroidal mode number) for the corresponding cases. The use of the term "mode number" may be somewhat misleading here, since the signal correlation was poor for two probes 90° toroidally around the machine; the ratio is inferred from wavelength measurements.

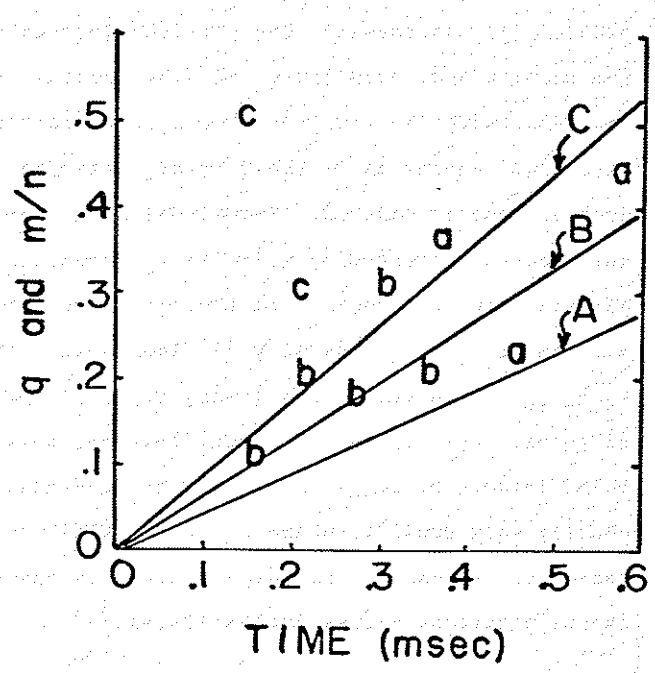

The fact that the fluctuations are very large even at very low values of plasma current seems somewhat surprising at first. However, as the plasma current is reduced by decreasing the poloidal loop voltage V_{TG}, the density and temperature of the plasma are also reduced, with the result that a larger fraction of the electrons' energy is in the form of streaming motion as loop voltage is reduced. Figure 6-6 shows the ratio of the electrons' streaming velocity $v_d = j/nef_{ut}$ to the electron thermal speed in the bridge region. In the midplane the current density is lower and the ratio $v_d/v_{e\ th}$ is therefore also lower, typically by a factor of three. Even in the midplane, however, this ratio is quite large. By comparison, in a tokamak this ratio is usually very small[6], on the order of 0.01. The high ratio of streaming to thermal speed is favorable for exciting current-driven instabilities.[7,8]

Another factor which may contribute to the instabilities is the low shear in the region where the plasma current flows. This is shown in Figure 6-7, which shows the safety factor q as a function of flux surface Ψ. The small slope in the region near $\Psi = 7$, where the current peaks, corresponds to small shear.

Figure 6-6. Typical ratio of electron streaming velocity v_d to electron thermal speed. The streaming velocity is obtained from $v_d = j/nef_{ut}$ and is shown for the bridge region; v_d is lower in the midplane since j is smaller there.

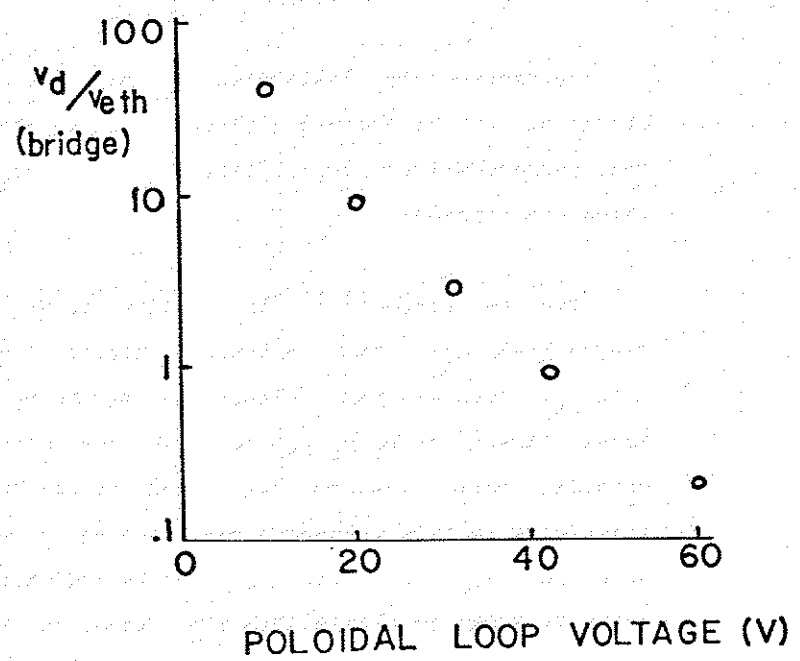

Figure 6-7. Safety factor q as a function of flux surface Ψ for various values of $\alpha = B_T/B_P)_{MPOW}$. The values shown are calculated for the vacuum fields; nowever, the plasma current contribution is negligible for the range of α's shown.

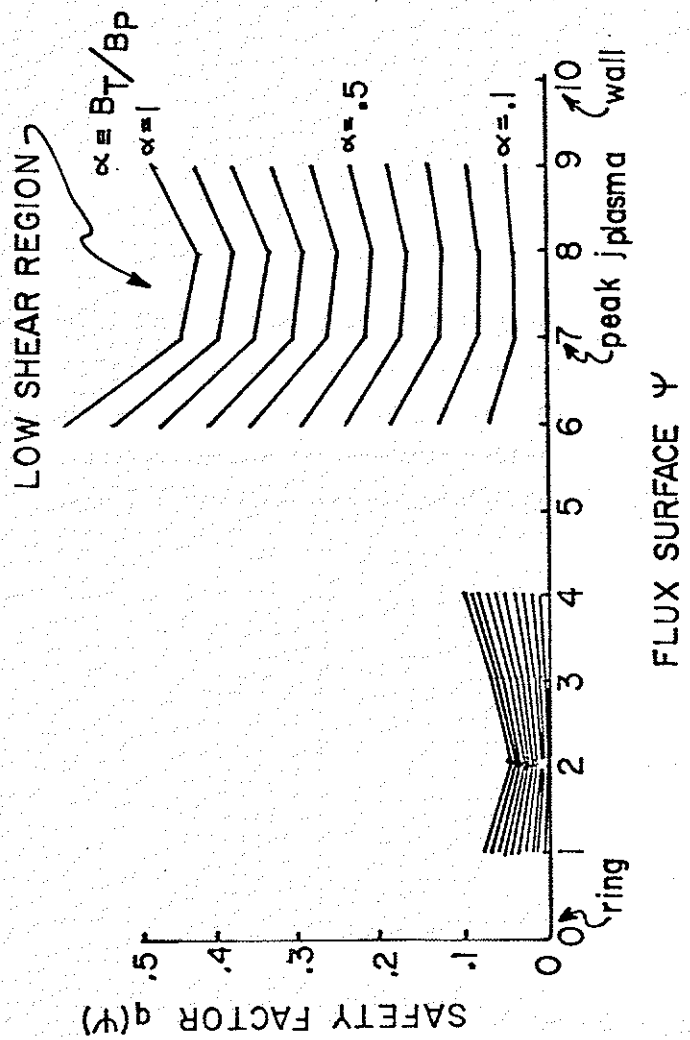

Since shear usually has a stabilizing effect,[3,9,10,11] it is unfortunate that the current peaks in the region of minimum shear.

C. CURRENT-DRIVEN INSTABILITIES

Current-driven instabilities may be grouped according to the frequency ranges in which they occur. Most current-driven instabilities fall into one of three broad ranges.

The two-stream[11,12] instability occurs at high frequencies near the electron plasma frequency, $\omega \sim \omega_{pe}$. Since this instability may be excited for large values[12] of $v_d/v_{e\ th}$ such as are produced by poloidal ohmic heating, we looked for radiation from the plasma in this frequency range using a microwave horn and diode detector sensitive to radiation in the range f= 7 GHz to f = 10 GHz; the detection apparatus is similar to that used by others to detect the two-stream instability.[14] Firing the 10 kW 8.8 GHz preionization pulse gave a rough sensitivity calibration which indicated that we could detect

radiated power levels greater than a few hundred watts. We varied the plasma density from $\sim 10^{11}$ cm^{-3} to $\sim 10^{13}$ cm^{-3}, corresponding to $f_{pe} \sim 2.8$ GHz to $f_{pe} \sim 28$ GHz, but no microwave radiation was observed on the diode detector. Thus we have seen no evidence for gross fluctuations in the frequency range near ω_{pe}.

Current-driven instabilities which fall into the intermediate frequency range near the ion cyclotron frequency $\omega = \omega_{ci}$ include the current-driven ion-cyclotron[14] instability. For these experiments the ion cyclotron frequency is typically a few MHz. If the external circuit has good frequency response, probes biased to collect ion saturation current have an upper frequency limit[15] of $\sim \omega_{pi} = \sqrt{ne^2/\epsilon_o M_i}$, which is in the range of tens of MHz to hundreds of MHz for our plasmas; however, no plasma activity in this frequency range has been observed on Langmuir probes during poloidal ohmic heating.

Thus there is no evidence that poloidal ohmic heating excites instabilities except those in the low-frequency range, near the drift frequency $\omega \sim \omega_*$. Candidates in this range include both

microinstabilities (ion-acoustic instability and current-driven drift instability) and MHD instabilities (rippling mode, tearing mode). While the author's bias is towards the former, the evidence to support this is not conclusive.

Drift waves[6,10,17-20] acquire their energy from plasma particles which are drifting perpendicular to a magnetic field due to gradients in temperature, density, or magnetic field; in addition, drift waves with $\vec{k} \cdot \vec{B} \neq 0$ can tap energy from particles streaming along the field. The wave propagation velocity across the field is on the order of the electron drift velocity, which is

$$v_* = \frac{kT_e}{eB} \frac{1}{n} \frac{dn}{dx} = \frac{\omega^*}{k_\perp}$$

for drifts induced by an electron density gradient dn/dx.

In order to couple energy from the electron current, i.e. from the electrons' streaming velocity v_d, the drift wave must have a component along the magnetic field, $\vec{k} \cdot \vec{B} \neq 0$; such waves are called oblique drift waves.[6,10,17,20] Kadomtsev[17] obtains from a fluid equation analysis the dispersion relation for the longitudinal part of such waves as

$$\omega_* \omega + \omega^2 - k_{\parallel}^2 c_s^2 = 0$$

where $k_{\parallel} = \vec{k} \cdot \vec{B}$, $c_s = \sqrt{\frac{kT_e}{M_i}}$ is the acoustic velocity (T_i is assumed = 0), the plasma β is assumed $< m_e/M_i$, and drifts due to $\vec{\nabla} T_e$, field curvature, etc. have been ignored. This is sketched in Figure 6-8. There are two branches, both of which become ion-acoustic waves at large $k_{\parallel}$. The accelerated wave has a perpendicular component which propagates in the electron diamagnetic drift direction; the retarded wave's perpendicular component propagates in the opposite direction. For small $k_{\parallel}$ the perpendicular component of the accelerated wave propagates with a phase velocity $\omega/k_{\perp} \sim v_*$. An analysis based on the Vlasov equation[10]

Figure 6-8. Dispersion relation for current-driven drift waves (From Reference 17).

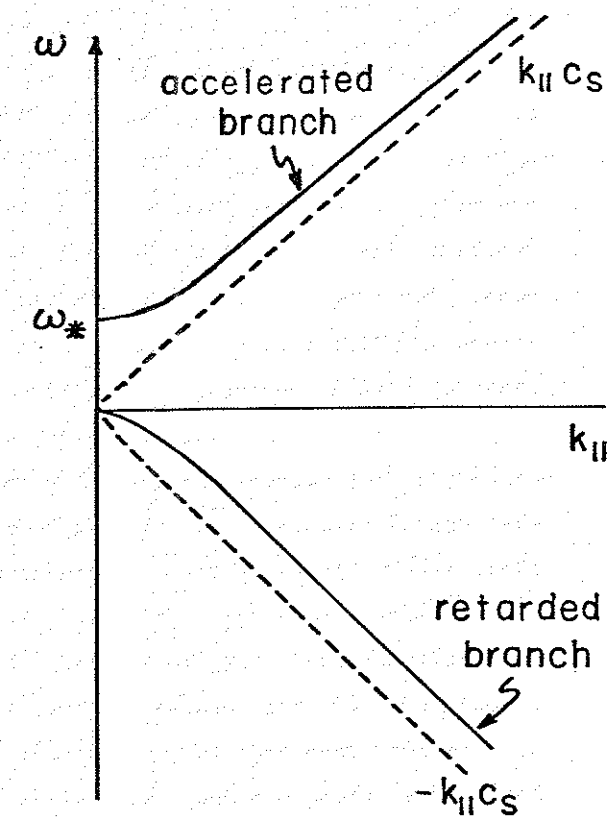

shows that the phase velocity of the component parallel to B must exceed the ion thermal velocity in order to avoid ion Landau damping, and be less than the electron streaming velocity in order to acquire energy from the electron current. If the plasma β is small the growth rate of the instability[19] increases with $k_\perp \rho_i$. A calculation[20] based on the Vlasov equation which numerically solves the radial eigenvalue problem for current-driven drift waves including a sheared magnetic field predicts that the minimum electron streaming velocity for instability is

$$v_d = v_{i\ th} \frac{4}{\sqrt{\pi}} \left(\frac{L_n}{L_s}\right) \frac{M_i}{m_e}$$

where $v_{i\ th}$ is the ion thermal speed, $1/L_n = \frac{1}{n}\frac{dn}{dx}$, and L_s is the shear length of the magnetic field, although in some experiments[30] current-driven drift waves have been seen at lower streaming speeds, typically $v_d \sim v_{i\ th}$. Plasma temperature gradients may also drive drift waves; the temperature gradients for the poloidal ohmic plasmas are not well known.

Typical parameters during poloidal ohmic heating include density scale lengths on the order of 10 cm, electron temperatures $T_e \sim 25$ eV, and magnetic fields $B \sim 1$ kG. This yields an electron diamagnetic drift velocity $v_* \sim 2.5 \times 10^5$ cm sec^{-1}, on the same order as the observed perpendicular phase velocity of the 5 to 10 kHz fluctuation peak $v_{\phi\perp} \sim 5 \times 10^3$ Hz x 20 cm = 10^5 cm sec^{-1}. If the ion temperature is a few eV, then the wave's parallel phase velocity must exceed a few times 10^6 cm sec^{-1} in order to be free from ion Landau damping. The parallel phase velocity of the wave is not well determined but exceeds 6×10^5 cm sec^{-1}. The direction of propagation of the observed wave perpendicular to B is in the electron diamagnetic drift direction, corresponding to the accelerated branch of the current-driven ion-acoustic drift instability. The shear length calculated from the maximum dq/dr in the current channel region in Figure 6-7 is around 75 cm, so that the threshold electron streaming speed for this instability should be at most $v_d \sim 10 \times v_{i\,th}$. This condition is almost certainly satisfied for all the poloidal ohmic discharges we have studied. Thus the fluctuation measurements are consistent with the

accelerated ion acoustic branch of a current-driven drift wave.

Current-driven MHD instabilities could also produce the observed low-frequency fluctuations. The persistence of the fluctuations at levels near 100% as the plasma current is reduced to a very small value suggests the instability is not an ideal kink-like mode. The strong externally-applied magnetic field should stabilize current-driven ideal MHD modes in the same way that a longitudinal magnetic field stabilizes a pinch: for a small enough plasma current the energy available from kinking the current channel is less than the energy required to bend the externally imposed field lines. In an ohmically-heated stellarator, which is similar to the octupole in that it has externally-applied poloidal and toroidal fields independent of the plasma current, such an ideal MHD mode is not expected to be unstable[21,22] when the rotational transform due to the plasma current is much smaller than the vacuum rotational transform. It is reasonable to suppose that a similar condition applies here. Resistive MHD instabilities, however, generally

have lower thresholds[22,23] and thus appear more likely to be responsible for the fluctuations.

Finite plasma resistivity becomes important in regions which are perturbed in such a way that $\vec{k} \cdot \vec{B} \sim 0$. Motion of the plasma across field lines is opposed by a restoring force

$$\vec{F} = \vec{J} \times \vec{B}_1 = \left(\frac{\vec{v} \times \vec{B}_1}{\eta}\right) \times \vec{B}_1$$

$$\text{where } \vec{B}_1 = \frac{\vec{k}\,(\vec{k} \cdot \vec{B})}{k^2}$$

For fluctuations with $\vec{k} \cdot \vec{B} \sim 0$ the numerator approaches zero and even a small resistivity allows the plasma motion to become decoupled from the field lines in these regions. The independent motion of field lines and plasma in the narrow region where $\vec{k} \cdot \vec{B} \sim 0$ can allow the plasma-field system to reach lower energy states which would be inaccessible if the plasma were a

perfect conductor. Outside this region the plasma motion is described by the ideal MHD equations.

The resistive MHD instabilities are the resistive interchange instability, the tearing mode, and the rippling mode. The first of these is a pressure-driven mode analogous to the ideal interchange mode. The tearing mode results from a current-density gradient in the $\vec{k} \cdot \vec{B} \sim 0$ layer; the field lines can break and reconnect into magnetic islands whose width can grow much larger than the thickness of the resistive layer. The competition between the energy obtained from this field line reconnection and the energy required to bend adjacent field lines requires that the unstable modes have a long wavelength,[24] i.e. the islands are long compared to their width. The rippling instability is typically a short wavelength mode and is driven by a local resistivity gradient; convective motion of the plasma creates a lower-resistivity channel where the current flows preferentially, which in turn enhances the convection. This mode can be stabilized by parallel electron heat conduction[25] and is believed to be stabilized for $T_e >$ 25 to 50 eV. The rippling mode is believed responsible

for much of the turbulence and enhanced transport in the relatively cool edge region of tokamaks, while tearing modes are probably responsible for much of the sawtooth-like MHD activity in the main tokamak current channel.[26,27] Rippling modes may also have been seen in ohmically-heated stellarator experiments.[28]

Since resistive MHD instabilities involve a coupling between resistive diffusion of magnetic fields and ideal MHD activity, both τ_R and τ_A are important in characterizing the plasma. Here τ_R is the characteristic time for field lines to diffuse across a dimension on the order of the current channel width, and is < 100 μsec for the plasmas produced by poloidal ohmic heating (Chapter IV). The Alfvén time τ_A is the time in which ideal MHD disturbances propagate across the current channel, and is typically a few x 10^{-8} sec for these plasmas. The ratio of these times is the magnetic Reynolds number, $S = \tau_R / \tau_A$, and is thus on the order of 10^3 to 10^4. The growth rate for the rippling mode from linear theory is on the order of $\gamma_R \sim (ka)^{2/5} S^{2/5} / \tau_R$, while for the tearing mode $\gamma_T \sim (ka)^{-2/5} S^{2/5} / \tau_R$, with k the total wavenumber and a the width of the current channel.[24] For our

plasmas this gives a growth rate of ~ 3 x 10^5 sec^{-1} for both modes, large enough to be consistent with the observed fluctuations which have f < 10 kHz.

Resistive MHD modes are predicted[28,29] to rotate with the plasma electrons at the electron diamagnetic drift frequency ω_*. Thus our observed frequencies and wavelengths are consistent with resistive MHD modes as well as drift modes, and in general it is difficult to distinguish the two. Since $\vec{k} \cdot \vec{B}$ must be ~0 for resistive MHD modes, the fairly short correlation lengths we observe are consistent with these modes only if there are a number of modes present which individually have $\vec{k} \cdot \vec{B} \sim 0$ but which sum together to produce signals which appear unrelated at different points in the machine. While this is certainly possible,[25] it seems somewhat fortuitous. In the case of drift waves, the presence of driving terms other than the streaming electrons makes the requirement $\vec{k} \cdot \vec{B} \sim 0$ seem less rigid than it is for resistive MHD modes.

It may be possible to stabilize either of these modes by heating the plasma more gently. If a small amount of poloidal ohmic heating were applied to a pre-existing plasma of moderate density, $v_d/v_{e\ th}$ could be kept below the value required to excite current-driven drift instabilities. The higher initial conductivity would also reduce the width of the resistive layer and lower the growth rate for resistive MHD instabilities.

REFERENCES FOR CHAPTER SIX

1. M.W. Phillips, University of Wisconsin PLP 765 (1980)

2. W.B. Thompson, An Introduction to Plasma Physics (Oxford : Pergamon Press, 1962)

3. G. Bateman, MHD Instabilities (Cambridge : MIT Press, 1978)

4. M.N. Rosenbluth and C. L. Longmire, Ann. Phys. 1, 120 (1957)

5. E.A. Rose, University of Wisconsin PLP 759a (1980)

6. C.R. DeVore, Nuc. Fus. 21, 105 (1981)

7. D.F. Smith and J.V. Hollweg, J. Plasma Phys. 17, 105 (1977)

8. J.M. Kindel and C.F. Kennel, J. Geophys. Res. 76, 3055 (1971)

*What is the poloidal resistivity? Do the magnetic mirrors enhance it above Spitzer resistivity as expected from mirror-enhanced resistivity theory?

In collisional plasmas the resistivity is $\eta \sim \eta_{Spitzer}$; as the collisionality is reduced the resistivity increases up to $\sim 1500 \times \eta_{Spitzer}$. The resistivity scales as $\sqrt{T_e}/n_e$ as expected from the mirror-enhanced resistivity theory of Lencioni and others. As the plasma collisionality becomes very small, the resistivity continues to increase; this is believed due to fluctuations and agrees with the observations of Lencioni and others.

*Is the input power converted to thermal plasma energy?

Measurements of T_e from triple Langmuir probes and from impurity line ratios, combined with microwave interferometer density measurements, show that the plasma energy content remains fairly low, with $T_e \lesssim 30$ eV and $n_e \sim 10^{13}$ cm^{-3}, compared with $T_e \sim 120$ eV, $n_e \sim 10^{13}$ cm^{-3} produced by the lower ohmic input power of

tokamak operation. Impurity radiation does not account for a significant fraction of the power loss.

*What is the poloidal current limit?

No obvious current limit has been seen; the plasma is noisy and has poor confinement throughout the range of currents studied.

*Does poloidal ohmic heating alter the multipole's equilibrium or stability?

An equilibrium code which solves the Grad-Shafranov equation shows that the measured poloidal plasma current does not significantly perturb the octupole equilibrium. The fluctuations persist even at small plasma currents where ideal MHD stability is probably not upset. Most of the fluctuation energy is in frequencies below f = 10 kHz; the fluctuations have a long wavelength parallel to B and a perpendicular wavelength of a few tens of cm. This is consistent with both drift instabilities and resistive MHD instabilities. The high ratio of $v_d/v_{e\ th}$ and the short correlation length of the fluctuations may be

evidence in favor of drift instabilities. The fluctuations enhance transport by a factor of two to five.

*Does poloidal ohmic heating produce other loss enhancement over a standard multipole configuration?

The one-dimensional transport code TEVOL indicates that for diffusion which scales classically, peaking the input power at $\Psi = 7$ leads to energy confinement times five to ten times worse than for a standard octupole configuration with the energy peaked on the separatrix. The effect is somewhat less pronounced if the diffusion obeys Bohm scaling, but in any case it is unfortunate that most of the power is deposited near the wall of the vacuum tank.

B. FURTHER WORK

The poloidal ohmic heating experiments we have done suggest several areas for future effort. More work is needed to understand the instabilities which cause the fluctuations. At present this is difficult

in part because the current which apparently drives the instability also produces and heats the plasma. If a fairly dense plasma could be produced by some other means it might be possible to observe a threshold for the instability and to determine the dependence of this threshold on other parameters, which could be useful in understanding the instability.

A coaxial plasma gun source will be added to Tokapole II in the near future and should provide the fairly dense initial plasma needed to investigate these ideas.

If the fluctuations are caused by current-driven drift waves, the gun plasma should make it possible to observe an instability threshold by varying the ohmic heating current. The instability should turn on at an electron streaming velocity between $v_d \sim v_{i\ th}$ and $v_d \sim 10 \times v_{i\ th}$. Reasonable parameters to expect from a gun source are $n_e \sim 10^{13}$ cm^{-3}, $T_i \sim T_e \sim 10$ eV, so that $v_{i\ th} \sim 5 \times 10^6$ cm/sec and $j \sim .8$ A/cm^2 to 8 A/cm^2 at the instability threshold. At this current density in the bridge region, the poloidal plasma current is $\sim$ 100 A to $\sim$ 1 kA (assuming the current density profile

has the same shape as in the present experiments.) The $\Delta\dot{B}_T$ technique can measure currents greater than a few hundred amperes with reasonable accuracy, so this should fall in a convenient range for measurement. For these parameters $\lambda_{Sp} \sim L_m$ so $\eta \sim 5\ \eta_{Sp}$; the resistivity calculations in Chapter Four then imply a poloidal bank voltage of ~ 200 V to ~1500 V at the instability threshold. Thus the gun should provide convenient parameters for observing the drift instability threshold. The prediction of threshold parameters for resistive MHD instabilities is more difficult and remains an area for future work.

The ability to produce the plasma independently of the poloidal ohmic heating might also lead to the ability to couple significant amounts of power to the plasma without enhancing the transport due to fluctuations: it might be possible to heat the plasma gently enough so that the diffusion coefficient would not be significantly increased. For the gun-produced plasma considered above, the ohmic power input at $v_d = 10 \times v_{i\ th}$ should be ~ 750 kW, sufficient to maintain the plasma energy if $\tau_E \sim 30\ \mu$sec. In the absence of fluctuations τ_E may be somewhat higher than

this, so it is reasonable to hope for significant heating in this case. Heating efficiency would probably remain poor due to the location of the plasma current.

At very high poloidal ohmic input powers, the energy confinement time appears to be decreasing; further work is needed to understand this. A careful study of the MHD stability properties of a multipole with poloidal currents might also be useful.

C. IMPLICATIONS

While the enhanced fluctuations and reduced confinement observed in these experiments are discouraging, poloidal ohmic heating may still be useful for heating multipole plasmas. For present-day research multipoles, it may provide a simple way of increasing the temperature and density of plasmas that have been produced by other means. Experiments are currently underway[1] on the Wisconsin Levitated Octupole in which an oscillating toroidal magnetic field is used to heat a gun-produced plasma, with no obvious harmful

effects observed at low heating voltages. The simplicity of the method may make up for its inefficiency due to the power location near the walls.

For an experiment such as the POP design[2] discussed in Chapter I, it might be possible to produce the background plasma for neutral beam heating by simply providing enough poloidal ohmic power to overcome the fluctuation-enhanced losses. It is difficult to extrapolate the present experiments to this situation, especially in view of the apparently worsening energy confinement we see at the highest poloidal ohmic input powers; in addition, it must be shown that it is possible to transform the noisy, short-lived plasma produced in this way into a plasma with a lifetime long enough to be of interest in a POP device. If the diffusion constant is on the order of D_{Bohm}, then scaling from the present experiment implies an energy confinement time for poloidal ohmic heating in the proposed POP device at $n_e \sim 5 \times 10^{12}$ cm^{-3}, $T_e \sim$ 100 eV of $\tau_E \sim 150$ μsec. This implies a required power input of .8w/cm^3, a fairly large input for the plasma obtained. Furthermore, generating a

poorly-confined plasma near the walls of the vacuum vessel might lead to an enhanced impurity influx.

It also be possible to start the POP device with a plasma produced by a gun or by other means and gently heat it with poloidal currents to provide a background plasma suitable for neutral beam heating. Tests of poloidal ohmic heating on gun-produced plasmas in Tokapole II and in the Wisconsin Levitated Octupole should indicate whether providing a fairly dense initial plasma makes poloidal ohmic heating a feasible technique. The further level of complication that this implies and the inefficiency due to the input power location remain unattractive features of this heating method.

REFERENCES FOR CHAPTER SEVEN

1. A. Kellman, private communication

2. University of California at Los Angeles, University of Wisconsin, TRW Defense and Space Systems Group, "A Proof-of-Principle of the Advanced Fuels Multipole-Surmac Concept," prepared for the Department of Energy, Office of Magnetic Fusion Energy (October 1978)